

**EFFICIENT SEISMIC IMAGING OF  
HEXAGONALLY SAMPLED DATA**

BY

**MOHAMMED SHAHABUDDIN**

A Thesis Presented to the  
DEANSHIP OF GRADUATE STUDIES

**KING FAHD UNIVERSITY OF PETROLEUM & MINERALS**

DHAHRAN, SAUDI ARABIA

In Partial Fulfillment of the  
Requirements for the Degree of

**MASTER OF SCIENCE**

In  
**ELECTRICAL ENGINEERING**

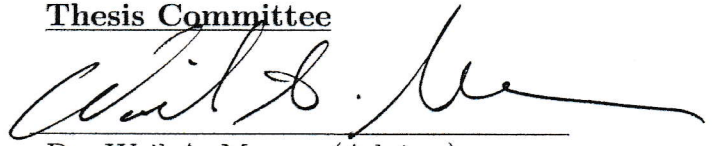
DECEMBER 2015

KING FAHD UNIVERSITY OF PETROLEUM & MINERALS  
DHAHRAN 31261, SAUDI ARABIA

DEANSHIP OF GRADUATE STUDIES

This thesis, written by **MOHAMMED SHAHABUDDIN** under the direction of his thesis adviser and approved by his thesis committee, has been presented to and accepted by the Dean of Graduate Studies, in partial fulfillment of the requirements for the degree of **MASTER OF SCIENCE IN ELECTRICAL ENGINEERING**.

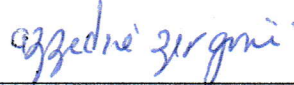
Thesis Committee



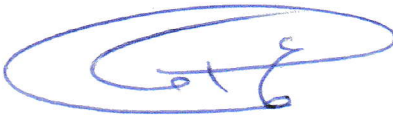
Dr. Wail A. Mousa (Adviser)




Dr. Abdellatif Al-Shuhail (Member)



Dr. Azzedine Zerguine (Member)



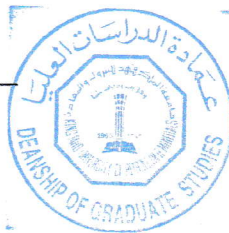
Dr. Ali A. Al-Shaiki  
Department Chairman



Dr. Salam A. Zummo  
Dean of Graduate Studies

Date

10/3/16



©Mohammed Shahabuddin  
2015

*Dedication*

To my beloved father,  
who always strived for excellence  
in education

# ACKNOWLEDGMENTS

*In the name of Allah, The Compassionate The Merciful*

*I would like to thank Allah (S.W.T) for His mercy and compassion, peace and blessing be upon His messenger the last Prophet Mohammad (p.b.u.h).*

*I would like to thank my advisor Dr. Wail A. Mousa for his guidance and direction throughout this master thesis, it was his passion that motivated me to finish this master's thesis. I thank my committee members Dr. Azzedine Zerguine, Professor, EE Dept. and Dr. Abdellatif Al-Shuhail, Associate Professor, ES Dept. for their constructive support. I want to express my gratitude to Dr. Abdellatif Al-Shuhail, Dr. Saleh Al-Dossary (Saudi Aramco) and Dr. Gino Ananos (Saudi Aramco) for providing the quintessential dataset for this research.*

*The financial support provided by the King Fahd University of Petroleum & Minerals is greatly appreciated. I have to thank Dr. Ali Al-Shaiki, Chairman EE Dept. for providing the much needed support at the apt time.*

*I would like to pay my gratitude to my beloved father, may Allah accept*

*him and grant him place in Jannat-ul-Firdous, for all the love and care he provided. I would like to thank my beloved mother, for her patience, when her only son wasn't around. I pray to Allah the Almighty to bless her with constant happiness, health and long life. I have to thank my sisters for their persuasion and love throughout my life, without their motivation I wouldn't have joined the M.S. program. My deepest gratitude to my uncle Mr. Mirza Ghouse Baig, CE Dept. KFUPM for his guidance and knowledge.*

*Finally I would like to thank Mr. Yahiya Naveed for being a mentor and friend throughout my stay at KFUPM. Special thanks to Mr. Haroon Ashraf, who did the hard work of creating basic and essential codes for hexagonal processing. I thank all the member of the Seismic Exploration and Analysis (SEA) Group for their suggestions and contributions towards this thesis.*

*Last but not the least, I thank my friends here at KFUPM, they're the family away from home. I would like to pass my gratitude to all my friends in my country for being there when I needed them the most.*

# TABLE OF CONTENTS

<b>ACKNOWLEDGEMENTS</b>	<b>v</b>
<b>LIST OF TABLES</b>	<b>ix</b>
<b>LIST OF FIGURES</b>	<b>x</b>
<b>ABSTRACT (ENGLISH)</b>	<b>xv</b>
<b>ABSTRACT (ARABIC)</b>	<b>xvii</b>
<b>CHAPTER 1 INTRODUCTION</b>	<b>1</b>
1.1 Thesis Contributions . . . . .	3
1.2 Thesis Organization . . . . .	4
<b>CHAPTER 2 BACKGROUND</b>	<b>6</b>
2.1 Introduction . . . . .	6
2.2 Reflection Seismology . . . . .	6
2.3 Land/Marine Acquisition . . . . .	7
2.3.1 2D vs 3D Seismic Acquisition . . . . .	8
2.4 Seismic Migration . . . . .	9
2.5 Migration Principle . . . . .	11
2.6 Seismic Imaging Techniques . . . . .	15
2.6.1 Phase Shift plus Interpolation (PSPI) Technique . . . . .	17
2.6.2 The PSPI Algorithm . . . . .	18
2.6.3 Simulation Results . . . . .	24

2.7	Hexagonal Data processing . . . . .	31
2.7.1	Hexagonal Data Handling . . . . .	32
2.8	Summary . . . . .	40
<b>CHAPTER 3 HEXAGONAL PHASE SHIFT PLUS INTERPOLATION WITH HEXAGONALLY SAMPLED DATA</b>		<b>41</b>
3.1	Introduction . . . . .	41
3.2	Spiral Architecture (SA) . . . . .	43
3.3	3D Hexagonal Phase Shift Plus Interpolation (HPSPI) in SA . . .	47
3.4	The Computational Complexity of HPSPI in SA . . . . .	50
3.5	Simulation Results . . . . .	50
3.5.1	The 3D seismic migration synthetic experiments . . . . .	50
3.5.2	Application to 3D SEG/EAGE salt model . . . . .	51
3.6	Discussions . . . . .	64
3.7	Conclusions . . . . .	66
<b>CHAPTER 4 3D DEPTH MIGRATION USING MCCLELLAN TRANSFORMATION IN SPIRAL ARCHITECTURE</b>		<b>67</b>
4.1	Introduction . . . . .	67
4.2	3D Seismic Imaging using 2D FIR Filters in SA . . . . .	70
4.3	Simulation Results . . . . .	73
4.4	Conclusions . . . . .	80
<b>CHAPTER 5 CONCLUSIONS</b>		<b>81</b>
5.1	Future Works . . . . .	82
<b>REFERENCES</b>		<b>83</b>
<b>VITAE</b>		<b>92</b>



# LIST OF TABLES

2.1	Sampling efficiency comparison for the three monohedral tiling. . .	34
3.1	Comparison of number of flops (for the complex multiplications, real-complex multiplications and complex additions) at a depth slice of stacked data for migrating the 3D SEG/EAGE salt model, using rectangular and hexagonal PSPI methods (with 200 reference velocities and 2048 fourier transform points). . . . .	53

# LIST OF FIGURES

2.1	Exploration Seismology. . . . .	7
2.2	Project economics comparison for seismic survey with 3D and without 3D. The higher probability of success in a 3D survey reduces the costs by reducing the number of wells drilled (courtesy of [1]).	9
2.3	An out-of-plane diffractor in 2D vs 3D, the data in the red traces provides the unambiguous direction and position of the diffractor (courtesy of [2]). . . . .	10
2.4	Typical 3D land acquisition layout using rectangular grids (courtesy of [1]). . . . .	10
2.5	Huygens Principle (modified after [3]). . . . .	12
2.6	The apparent dip with a dip angle $\beta$ when migrated moves up-dip (courtesy of [3]). . . . .	14
2.7	Various seismic imaging techniques. . . . .	16
2.8	The Phase Shift Plus Interpolation (PSPI) algorithm. . . . .	20
2.9	Inline section (69) of (a) SEG/EAGE salt model, (b) Migration result using rectangular phase shift plus interpolation. . . . .	25
2.10	Inline section (99) of (a) SEG/EAGE salt model, (b) Migration result using rectangular phase shift plus interpolation. . . . .	26
2.11	Crossline section (87) of (a) SEG/EAGE salt model, (b) Migration result using rectangular phase shift plus interpolation. . . . .	27
2.12	Crossline section (126) of (a) SEG/EAGE salt model, (b) Migration result using rectangular phase shift plus interpolation. . . . .	28

2.13	Depth section (29) of (a) SEG/EAGE salt model, (b) Migration result using rectangular phase shift plus interpolation. . . . .	29
2.14	Depth section (43) of (a) SEG/EAGE salt model, (b) Migration result using rectangular phase shift plus interpolation. . . . .	30
2.15	Types of monohedral tiling (a) triangular, (b) rectangular and (c) hexagonal, covering the Euclidean plane regularly without gaps. . .	33
2.16	(a) square with 8 folds of symmetry, (b) hexagon with 12 folds of symmetry (courtesy of [4]). . . . .	35
2.17	a circularly band limited signal inscribed in (a) square and (b) hexagon. Inaccurate representation of circle is 27.3% and 10.2% by square and hexagon respectively. (courtesy of [5]). . . . .	36
2.18	Seismic band region (a) In the $k_x - k_y - \omega$ space, (b) In the $k - \omega$ plane and (c) in the $k_x - k_y$ plane (courtesy of [6]). . . . .	37
2.19	Shows (a) hexagonal acquisition layout using rectangular bins, (b) zoomed layout. The shot locations are represented by squares and receiver by circles (courtesy of [1]). . . . .	38
2.20	Hexagonal acquisition layout using hexagonal bins (courtesy of [6]).	39
2.21	Hexagonal indexing in the $B_h$ coordinate system for aggregate level 0, 1 and 2 (courtesy of [4]). . . . .	39
3.1	(a) 2D data representation in spiral architecture, (b) stored as 1D vector (courtesy of [7]). . . . .	45
3.2	(a) 3D data representation in spiral architecture, (b) stored as 2D array (Modified after [7]). . . . .	46
3.3	Flow chart of Hexagonal Phase Shift Plus Interpolation. . . . .	48

3.4	Impulse response comparison of RPSPI with HPSPI, with $\Delta z = 2m$ , $\Delta x = 10m$ , $\Delta y = 10m$ , $\Delta t = 4ms$ , and $c = 1000m/s$ . The maximum frequency is 50 Hz using (a) In-line section of impulse response migrated using rectangular PSPI, (b) In-line section of impulse response migrated using hexagonal PSPI, (c) and (d) show the depth slices of migrated image using rectangular PSPI and hexagonal PSPI respectively. . . . .	52
3.5	Inline section of SEG/EAGE salt model (a) original, (b) hexagonally sampled, (c) migrated section using rectangular PSPI, (d) migrated section using hexagonal PSPI in SA. . . . .	54
3.6	Inline section of SEG/EAGE salt model (a) original, (b) hexagonally sampled, (c) migrated section using rectangular PSPI, (d) migrated section using hexagonal PSPI in SA. . . . .	55
3.7	Crossline section of SEG/EAGE salt model (a) original, (b) hexagonally sampled, (c) migrated section using rectangular PSPI, (d) migrated section using hexagonal PSPI in SA. . . . .	56
3.8	Crossline section of SEG/EAGE salt model (a) original, (b) hexagonally sampled, (c) migrated section using rectangular PSPI, (d) migrated section using hexagonal PSPI in SA. . . . .	57
3.9	Depth section of SEG/EAGE salt model (a) original, (b) hexagonally sampled, (c) migrated section using rectangular PSPI, (d) migrated section using hexagonal PSPI in SA. . . . .	58
3.10	Depth section of SEG/EAGE salt model (a) original, (b) hexagonally sampled, (c) migrated section using rectangular PSPI, (d) migrated section using hexagonal PSPI in SA. . . . .	59
3.11	Challenging parts of the depth slice of SEG/EAGE salt model are highlighted by rectangles. The rectangle on top and bottom will be referred as box-1 and box-2 respectively. . . . .	60

3.12	Zoomed area SEG/EAGE salt model, (a) – (b) rectangular velocity model for box-1 and box-2, (c) – (d) migrated section using rectangular PSPI, (e) – (f) migrated section using hexagonal PSPI in SA. It can be observed that hexagonal PSPI represent curves much better than rectangular version. . . . .	61
3.13	Challenging parts of the depth slice of SEG/EAGE salt model are highlighted by rectangles. The rectangle on top and bottom will be referred as box-1 and box-2 respectively. . . . .	62
3.14	Zoomed area SEG/EAGE salt model (a) – (b) rectangular velocity model for box-1 and box-2, (c) – (d) migrated section using rectangular PSPI, (e) – (f) migrated section using hexagonal PSPI in SA. . . . .	63
3.15	Cross-line section of SEG/EAGE salt model (a) original, (b) hexagonally sampled, (c) zoomed section of the original model, (d) zoomed section of hexagonally sampled model. The hexagonally sampled model is smeared and blurred, as the rectangular model is of low resolution. . . . .	65
4.1	Chebyshev structure for designing 2-D FIR digital filters from 1-D odd length filters (courtesy of [8]). . . . .	71
4.2	Hale’s McClellan transformation filter for rectangular grids (a) original, (b) improved, where $c \approx 0.0255$ (courtesy of [9]). . . . .	74
4.3	Hedley’s McClellan transformation filter for hexagonal grids (a) original, (b) improved, where $a \approx -0.708$ , $b \approx 0.454$ , $c \approx -0.00942$ and $d \approx 0.00692$ (courtesy of [10]). . . . .	75
4.4	Proposed McClellan transformation filter for hexagonal grids in SA (a) original, where $a \approx -0.333$ , $b \approx 0.222$ , (b) improved, where $a \approx -0.354$ , $b \approx 0.227$ , $c \approx -0.00471$ and $d \approx 0.00346$ . . . . .	76
4.5	Depth slice of the 3D seismic migration of impulse response using Hale-McClellan transformation filter (a) original, (b) improved. . .	77

4.6	2D Filter response (a) improved McClellan transformation as in [9] , (b) proposed improved McClellan transformation in SA. . . . .	78
4.7	Depth slice of the 3D seismic migration of impulse response using proposed McClellan transformation filter in SA (a) original, (b) improved. . . . .	79

# THESIS ABSTRACT

**NAME:** Mohammed Shahabuddin  
**TITLE OF STUDY:** Efficient Seismic Imaging of Hexagonally Sampled Data  
**MAJOR FIELD:** Electrical Engineering  
**DATE OF DEGREE:** December 2015

*Natural resources such as oil and gas, hidden in subsurface structures are extremely important in our daily lives. In order to meet the demand it is required to employ higher resolution imaging techniques for better estimation of the reserves. Thus amount of data processing has increased exponentially. Hexagonally sampling serves as a solution, requiring lesser number of samples to represent same information. Seismic data is circularly band limited in the wave-number domain. Hexagonal spatial sampling is the optimum technique for seismic data. Researchers have proposed various methods to address hexagonal data cells, because of their non-orthogonal alignment. Spiral Architecture (SA) has proven to be the most optimal addressing scheme proposed for hexagonal data addressing. In this research, three dimensional (3D) post-stack depth imaging is performed using the Phase Shift Plus Interpolation (PSPI) technique for hexagonally sampled*

*data in Spiral Architecture (SA). The modified algorithm saves 80% computational time compared to the conventional rectangular approach. Further, another method of seismic imaging is explored. Two dimensional (2D) Hexagonal FIR filters are designed using McClellan Transformations. Since a hexagon is a better approximation to a circle, the designed hexagonal 2D filters have an improved response compared to the rectangular counterparts, besides the evident computational savings.*





## CHAPTER 1

# INTRODUCTION

The developments in the modern era, depend heavily on oil and gas resources to meet their energy requirements. These resources are buried deep down the earth surface and require drilling up to the depth of kilometres beneath the surface. This extraction process is very costly, thus, there is a need for an accurate estimation of the reserves. The seismic exploration process finds possible drilling locations for oil and gas. For oil production it is important to obtain a clear and accurate image of the subsurface [11, 12]. This can be done using a method called exploration seismology. This technique involves creating an artificial earthquake which sends the seismic waves down the earth surface. These waves are reflected at the boundaries of different layers in the subsurface. The reflections are recorded on the subsurface using recording devices such as geophones. There is a need to process this acquired seismic data, as the received data is effected by noise, thereby we use some digital signal processing techniques to improve the data [11, 13].

Digital signal processing has proven to be very useful in many fields such as sonar, radar, medical, communication, seismology etc. Seismic Imaging determines the structure of the interior of the earth from the data received at the surface.

The major constraints in seismic digital signal processing arise from the huge data acquired, in order to obtain high resolution imaging. The number of receiver lines to be used during the acquisition, has jumped from less than 100 in 1970 to about 200,000 receiver channels today. It is estimated to reach about 1 million by 2020 [14]. A typical seismic exploration data, now a days, is fully done in three-dimensions (3D), where the receivers are laid based on the rectangular grids. The seismic data usually would be in TeraBytes (TB's), spanning multiple hard disks.

Researchers in the past have found that two-dimensional (2D) hexagonal sampling is much efficient than the usual (2D) rectangular sampling and would require 13.4% fewer samples [15]. Hexagonal sampling has the alternate rows/columns placed half sample interval with respect to the other rows/columns and it has six equidistant neighbours and has natural symmetry. Hexagonal sampling offers the best approximation to circularly band limited signals, seismic signals in wavenumber domain are circularly band-limited and thus, it is

more appropriate to use hexagonal sampling than rectangular for seismic data acquisition. Eventually requiring lesser computational requirements and storage.

## 1.1 Thesis Contributions

The structural geometry of a hexagon is 50% more symmetric than a square, exhibiting a 12 fold symmetry compared to 8 fold symmetry of a rectangle. This is the primary reason for the efficiency of hexagonal sampling technique. Each pixel in a rectangular grid has four nearest neighbours and four diagonal neighbours, which are farther. While in a hexagonal grid each pixel will have six equidistant neighbours. This increases the sampling efficiency of a hexagonal grid.

Several attempts were made to employ the advantage of the hexagonal sampling in the field of image processing and seismic data processing, which employ the rectangular addressing techniques to deal with hexagonal data. These approaches achieve the savings in terms of number of samples processed, but the computational power requirement was high.

Spiral architecture (SA) for hexagonal data was proposed by Sheridan in 1996 [16]. SA introduces a special addressing algorithm, which uniquely identifies each hexagon of the structure with a base-7 index. This allows a 2D data to be represented in 1D, likewise a 3D data is represented as 2D.

In this thesis, we propose a 3D seismic migration technique based on the spiral architecture. This is a first attempt to deal with 3D seismic imaging algorithm using the spiral architecture. The computational efficiency of the hexagonal processing is explored. Phase Shift Plus Interpolation (PSPI) migration technique is used to image hexagonally sampled seismic data. The 3D PSPI in SA was tested using the impulse cube and more challenging 3D stacked SEG/EAGE seismic data set.

Computational cost of 3D explicit depth migration of seismic data is high. Another method to migrate 3D seismic data is by convolving spatially varying two-dimensional (2D) filters with the data for each angular frequency ( $\omega$ ). In this thesis an attempt is made to migrate the hexagonally sampled the seismic data using the McClellan transformation filters in SA. Again, this is tested on the synthetic data sets, in order to prove the spiral architecture concept.

## 1.2 Thesis Organization

This thesis is structured as follows, Chapter 2 provides an introduction and background of the seismic imaging techniques, where the PSPI technique is discussed in details. Also, the fundamental concepts of the spiral architecture are explained. Chapter 3 deals with the PSPI migration technique for the spiral architecture and the imaging results and efficiency of the algorithm are discussed. In Chapter 4, seismic imaging is performed as a filtering process using the McClellan transfor-

mation filters in spiral architecture. Finally, conclusions and future works are provided in Chapter 5.

## CHAPTER 2

# BACKGROUND

### 2.1 Introduction

This chapter deals with the concept of seismic exploration and analysis using traditional rectangular grids. The advantages of 3D seismic imaging over 2D are discussed. Hexagonal grid acquisition and its relevance to circularly band-limited seismic signals is explained. The data handling in hexagonal grid is explored using spiral architecture. Simulation results are shown for the existing techniques.

### 2.2 Reflection Seismology

Reflection seismology is the technique to estimate the properties of the subsurface of the earth using the principles of seismology. The seismic waves are produced by creating an artificial earthquake on the surface, these waves are reflected from various layers in the subsurface and the reflections are recorded at the surface using geophones. The process involves seismic acquisition, processing and interpretation

to obtain the subsurface image.

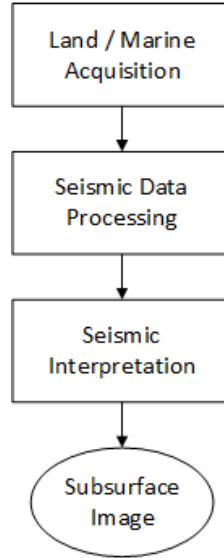


Figure 2.1: Exploration Seismology.

## 2.3 Land/Marine Acquisition

For a land acquisition, geophones are used as receivers, which are laid on the surface in lines at regular intervals called as receiver lines (denoted as  $x$ ), sources are shot in the cross-line direction (denoted as  $y$ ). During a marine acquisition, the receiver lines are called streamers, which has hydrophones located at regular intervals, floating on the water surface and can go 6-8 KM long. Air guns are used as sources in marine seismic. Multiple receiver lines can be laid at regular intervals leading to 3D seismic acquisition, while in a 2D acquisition only one receiver line is used.



### 2.3.1 2D vs 3D Seismic Acquisition

The increase in information and accuracy provided by 3D over the 2D seismic has propelled the industry to 3D seismology. Success ratios have increased for the oil companies by using 3D seismic. An increase in the success rate from 13% to 44% in just 5 years was reported by a large oil company in a world wide study by employing 3D seismology [17]. Even a small increase in the success ratio of drilling wells with a 3-D survey (e.g., 1:5) versus without a 3-D survey (e.g., 1:6) could justify the cost of a 3-D survey (Figure 2.2). Assume drilling 6 wells at a dry hole cost of \$500,000 each versus drilling 5 wells at a cost of \$500,000 each with 3-D data, it would still save \$500,000.

In a 2D seismic survey, the earth is assumed to be a cylinder, with its axis orthogonal to the survey, accuracy of the 2D survey depends on the fulfillment of this assumption. Whenever this assumption is not satisfied, the 2D seismic interpretation yields a distorted image. In Figure 2.3, the point diffractor  $R_{3D}$  is out of plane with respect to the 2D acquisition direction. It creates reflections that are incorrectly back-propagated in the earth along the vertical plane and imaged at wrong location  $R_{2D}$ . To correctly image, 3D imaging needs to be applied to back-propagate along the orthogonal plane.

A typical (rectangular) layout of 3D land acquisition is depicted in Figure 2.4. The receiver lines are represented as horizontal blue lines spaced at regular

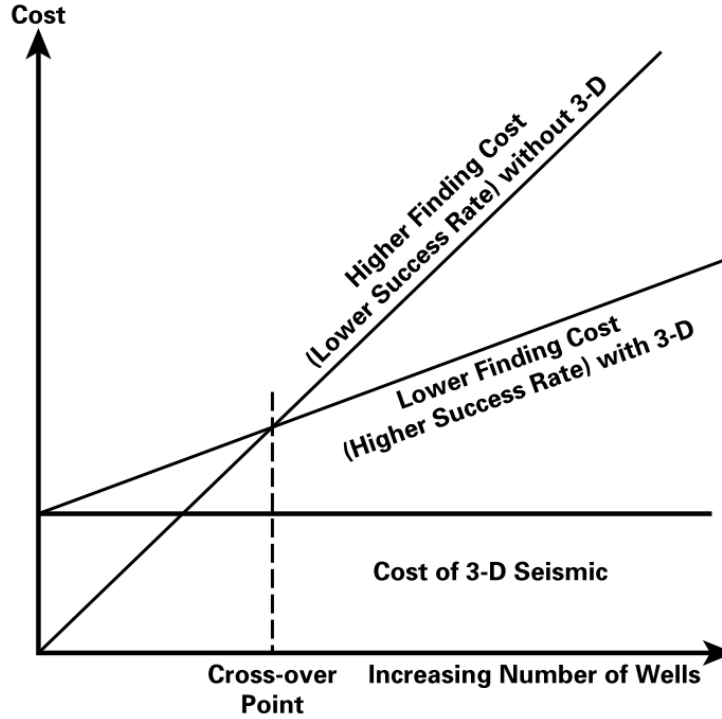


Figure 2.2: Project economics comparison for seismic survey with 3D and without 3D. The higher probability of success in a 3D survey reduces the costs by reducing the number of wells drilled (courtesy of [1]).

intervals, this spacing is called Receiver Interval (RI), while the source lines are represented by vertical red lines separated by Source Intervals (SI). Each receiver line is separated by Receiver Line Interval (RLI), while source lines are separated by Source Line Interval (SLI), more details are explained in [1].

## 2.4 Seismic Migration

Seismic migration is the process by which seismic events are geometrically re-located in either space or time to the location the event occurred in the subsurface, rather than the location that it was recorded at the surface, thereby creating a more accurate image of the subsurface. This process overcomes the limitations of

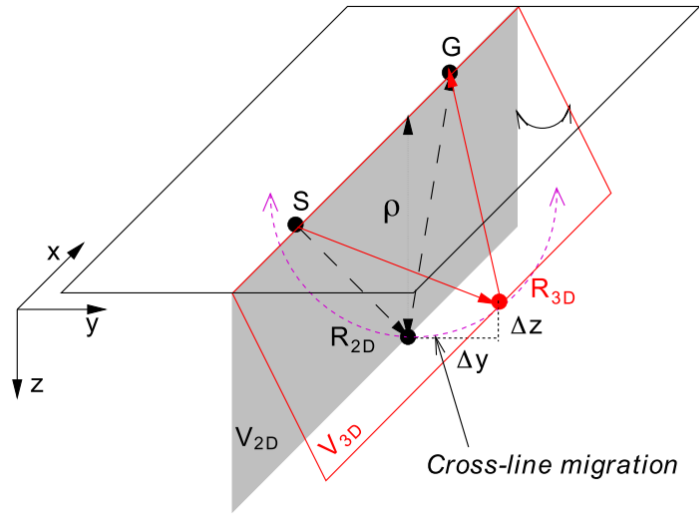


Figure 2.3: An out-of-plane diffractor in 2D vs 3D, the data in the red traces provides the unambiguous direction and position of the diffractor (courtesy of [2]).

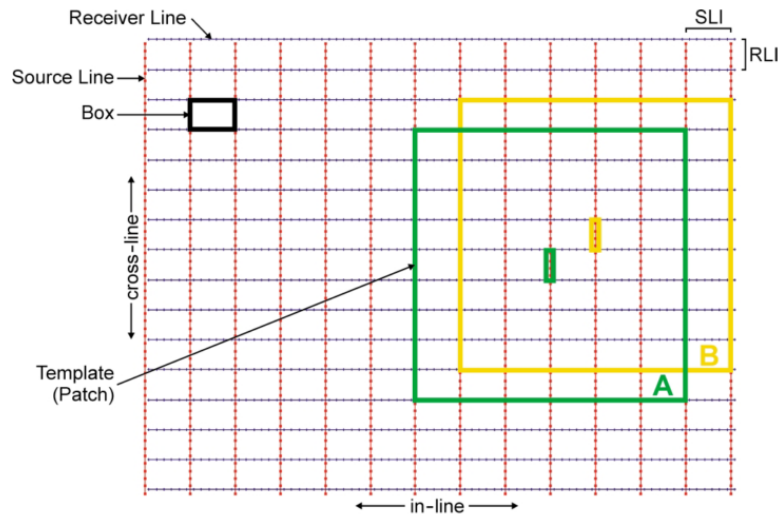


Figure 2.4: Typical 3D land acquisition layout using rectangular grids (courtesy of [1]).

geophysical methods restricted by areas of complex geology, such as: faults, salt bodies and folding.

## 2.5 Migration Principle

Huygens principle is the basis of migration [18]. This can be explained by the harbor example shown in Figure 2.5. Assume that a calm breeze is coming from the ocean and an observer is at the beach where a barrier that exists at a certain distance from the beach and has a gap (hole) for water to pass through. Then, one will observe that the gap on the barrier acts as a secondary source and has generated semi-circular wavefronts that are propagating towards the beach. Now, assume that we did not know about the barrier, we lay our receiver cables along the beach and record in time the approaching waves.

We apply the same principle into reflection seismology by imagining that each point in the geological interface acts as secondary source in response to incident wavefield. This is called the exploding reflector model [19]. Consider a point scattering in a medium as shown in Figure 2.5. The minimum travel time is given by:

$$t_o = \frac{2z}{v}, \quad (2.1)$$

where  $z$  the depth of scattering and  $v$  is the velocity of wave propagation. Now, we assume that the velocity is constant and the source and receiver are at the same location (zero-offset). The travel time as function of distance  $x$  can be given by [19]:

$$t(x) = \frac{2\sqrt{x^2 + z^2}}{v}. \quad (2.2)$$

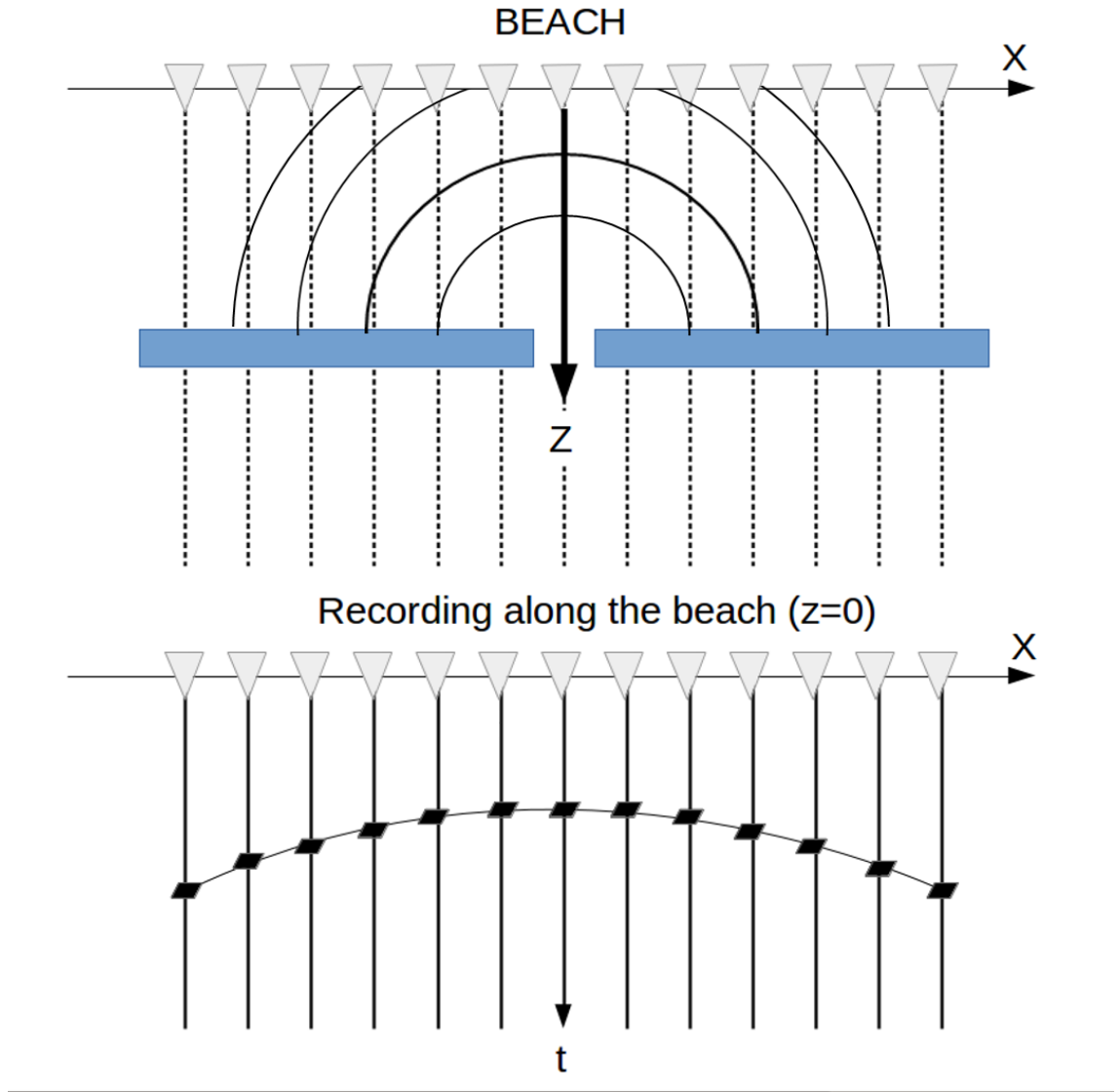


Figure 2.5: Huygens Principle (modified after [3]).

By squaring and substitution, we obtain:

$$\frac{t(x)^2}{t_0^2} - \frac{4x^2}{v^2 t_0^2} = 1. \quad (2.3)$$

This shows that the travel time curve for a scattered arrival has hyperbolic form with the apex directly pointing towards the secondary source as shown in

Figure 2.5.

Now if one considers a series of such scatter points in the barriers which generates diffraction hyperbolas. Following Huygens Principle, these hyperbolas sum coherently only at the time of reflection, while their later contribution's cancel out. However, if the reflector vanishes at some point there will be a diffracted arrival from the endpoint which will show up in the zero-offset data. This creates an artifact in the structure, which might be falsely interpreted as a structure. Hence, such sections requires migration in order to remove such artifacts.

Another important aim of migration is to map the apparent dip that is seen on the zero - offset to the true dip. The true dip angle is always greater than the apparent angle [20]. Consider a reflector at an angle of  $\theta$  to the earth as shown in Figure 2.6. The zero offset travel time for a wavefield propagating from distance  $x$  down to the reflector and back up again is given by  $t = 2r/v$ , where  $r$  is the wavefield path length and is equal to  $x \sin \theta$ . Now, to compare the apparent dip and the true dip we have to travel time to depth via Eq.(2.1). In the un-migrated depth section  $z = x \sin \theta$ , from Figure 2.6 one can obtain slope of the event, which is equal to the tangent of the apparent dip angle say  $\beta$ .

Therefore,

$$\tan \beta = \sin \theta. \quad (2.4)$$

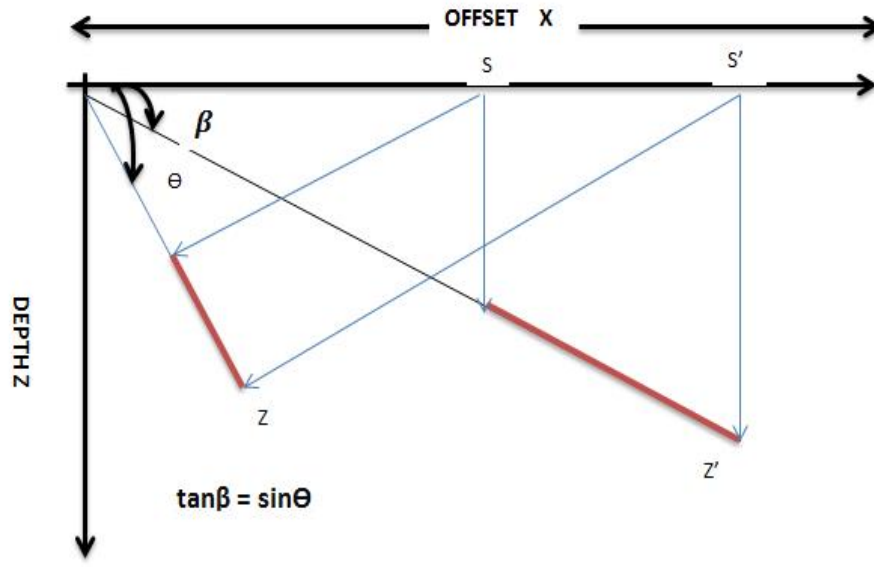


Figure 2.6: The apparent dip with a dip angle  $\beta$  when migrated moves up-dip (courtesy of [3]).

This shows that the apparent dip angle is always less than true angle. Hence, we can say that migration moves up dip the reflectors. In addition, the length of the reflector in the geological section is shorter than in the time section. Thus migration also shortens reflector. In short migration focuses energy by collapsing diffraction as well as it correctly shortens, steepens and moves reflectors up-dip. These are the main objectives of seismic imaging [21].

## 2.6 Seismic Imaging Techniques

There are many migration techniques that are available from the literature. In the early stages of reflection seismology, migration was performed by hand and it was called compass migration [3]. It was used by the interpreters before the computerized versions were available. Later on a new method was introduced by Karcher called Hagedoorn migration which was valid only for constant velocities [22]. It was simply relying on spreading the energy along the semicircles and let waveform reconstruction compose the reflector position, it however provides a valuable insight to the migration process [18]. Kirchhoff migration (summation operator) is considered to be the best but its implementation part varies from a very simple algorithm to one that is complex. This scheme sums the energy along the diffraction. The Fourier transform ( $F - K$ ) migration was introduced by Stolt in 1978 [23]. This method is ideal when it comes to constant velocities and will migrate accurately to 90 degrees. Finite difference method was introduced in order to find the data on  $(n + 1)^{th}$  layer based on  $n^{th}$  layer. Methods based on phase shift were developed by Gazdag by using 2-D Fourier transform. This method is appropriate for the depth migration. Phase shift migration [24] is unconditionally stable, which applies phase shift in Fourier domain to the extrapolated wave field [25, 24, 26, 27]. The main drawback of this method is that, it requires a constant velocity medium or a medium which is just a function of depth. Phase Shift plus interpolation (PSPI) is one of the forms of phase-shift method that allows lateral velocity changes. There are few techniques



available in the literature that works by switching their domains back and fourth by fixing one dimension in one particular domain. Figure 2.7 shows the flow chart of various imaging techniques.

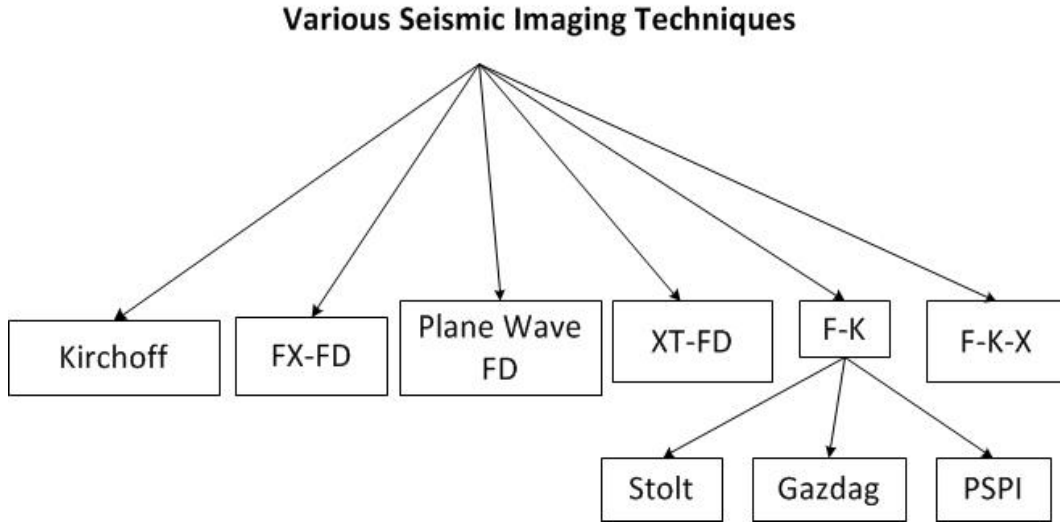


Figure 2.7: Various seismic imaging techniques.

Here, we start with the acoustic data in 3D, which is given as  $p(x, y, z, t)$  in a medium with a constant material density and velocity  $v$ . The following represents the partial differential equation (PDE) that governs the propagation of  $p(x, y, z, t)$  [24]:

$$\frac{\partial^2 p}{\partial x^2} + \frac{\partial^2 p}{\partial y^2} + \frac{\partial^2 p}{\partial z^2} = \frac{1}{v^2} \frac{\partial^2 p}{\partial t^2}, \quad (2.5)$$

where  $x$  is the crossline direction and  $y$  is the inline direction and  $z$  represents the depth direction and  $t$  is the time. The wavefield  $p(x, y, z, t)$  can be expressed in the frequency domain as follows:

$$p(x, y, z, t) = \int \int \int_{-\infty}^{+\infty} P(k_x, k_y, z, \omega) \exp[-i(\omega t - k_x x + k_y y)] dk_x dk_y d\omega, \quad (2.6)$$

where  $\omega$  is frequency and  $k_x$  and  $k_y$  are wavenumbers in  $x$  and  $y$  direction.

By substituting Eq.(2.6) in Eq.(2.5) we obtain:

$$\frac{\partial^2 P}{\partial z^2} = \left( \frac{\omega^2}{v^2} - k_x^2 - k_y^2 \right) P, \quad (2.7)$$

which holds true for all  $k_x$ ,  $k_y$  and  $\omega$ .

If  $v$  is constant, the solution to the above equation is given by:

$$P(k_x, k_y, z = \Delta z, \omega) = P(k_x, k_y, z = 0, \omega) e^{ik_z \Delta z}, \quad (2.8)$$

where

$$k_z = \pm \sqrt{\frac{\omega^2}{v^2} - k_x^2 - k_y^2}. \quad (2.9)$$

Equation 2.8 holds good for  $v(z)$  as long as  $\Delta z$  is small enough.

### 2.6.1 Phase Shift plus Interpolation (PSPI) Technique

In case of complex geological structures, where lateral velocities have considerable variations, the phase shift method of migration does not work well. Hence, a new method is introduced to incorporate the lateral velocity variations, called Phase Shift plus Interpolation (PSPI). In PSPI, we use a number of reference

velocities to extrapolate the wavefield to next depth. The accuracy of the obtained result depends upon the number of reference velocities used at each depth [28]. The basic idea of PSPI, is to select several reference velocities at each depth to account for the lateral velocity variations in each extrapolation step and obtain multi-reference wavefield in the frequency-wavenumber domain. Based on the relationship between local velocities and the reference velocities, we obtain a final image by interpolating the reference wavefield.

The important features of PSPI are:

- This method allows lateral velocity changes.
- This method computes a number of sub-layers at different velocities for the next depth level.
- Each new layer is inverse Fourier transformed into  $(\omega, x, y)$  domain sub layer.
- The output layer is interpolated from the different velocity sub-layers using the appropriate lateral velocity.
- The new layer is transformed back to the  $(\omega, k_x, k_y)$  domain for the next downward step.

The PSPI method is described more clearly by Gazdag [24].

### 2.6.2 The PSPI Algorithm

PSPI assumes that the wavefield at point  $(x_k, y_k)$  is equivalent to reference wave field as long as the velocity in this point  $v(k_x, k_y)$  equals to reference velocity  $v_i$ .

The implementation of PSPI involves three steps:

- Initial phase shift is applied to the wavefield.
- Phase shift is applied to set of reference wavefield using reference velocities.
- After we obtain these reference wavefield, we approximate  $P(x, y, z, \omega)$  by linearly interpolating over reference wave fields if  $v(k_x, k_y)$  is close to  $v_i$ .

The flow chart for the PSPI is shown in Figure 2.8 To maintain a high accuracy for small dip, laterally varying time-shift is applied in space frequency domain.

$$P(k_x, k_y, z, \omega) = P(x, y, z, \omega) e^{i\frac{\omega}{v(x,y)}\Delta z}. \quad (2.10)$$

This means that this extra time shift will be compensated later in  $(k-\omega)$  domain, i.e., the phase shift term now changes to  $e^{(ik_z\Delta z - i\frac{\omega}{v(x,y)}\Delta z)}$  instead of  $e^{ik_z\Delta z}$  when extrapolating to the next depth.

Two conditions degrade the performance of migration algorithm:

- Insufficient sampling of the data along the shot axis.
- Lateral velocity variations.

### The Computational Complexity for acoustic PSPI

The computational cost for imaging using PSPI using  $N_{FFT}$  FFT points and  $n_{ref}$  velocities at each depth slice is given by [24, 8].

For complex multiplications,

$$PSPI - COST_X = 2N_{FFT} \times n_{ref} + (n_{ref} + 2) \times \frac{N_{FFT}}{2} \log_2 N_{FFT}, \quad (2.11)$$

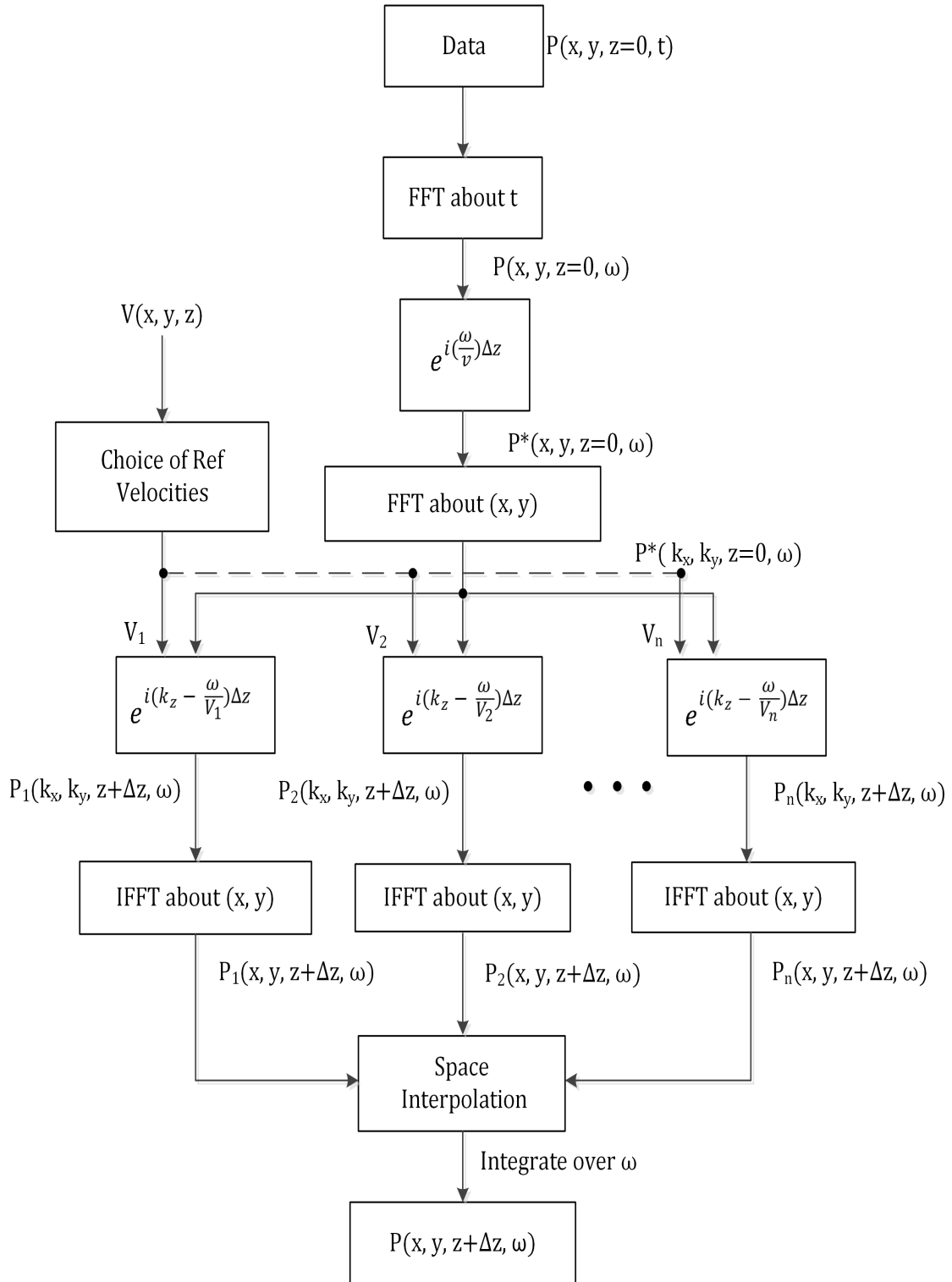


Figure 2.8: The Phase Shift Plus Interpolation (PSPI) algorithm.

For complex additions,

$$PSPI - COST_+ = (n_{ref} + 2) \times N_{FFT} \log_2 N_{FFT}. \quad (2.12)$$

In both cases, each complex multiplication requires six flops whereas, each complex addition requires two flops as given in [29].

### **Selection of Reference Velocities**

Selection of reference velocities is one of the important criteria in implementing PSPI technique. For efficient computation of depth imaging, there should be a minimum number of reference velocities. Also, for the accurate computation of the wavefield extrapolation the reference velocities should be close to the velocity model [30, 28, 31]. There are many methods that are available for selection of reference velocities like geometric progression method [31], statistical method [28], peak search method [28], etc. Here, we are going to discuss the two basic methods they are:

#### **Geometric Progression Method**

This method was introduced by Gazdag and Sguazzero [24]. In this method, the ratio of maximum and minimum velocity is found at some depth (let's say R). A factor called  $\rho$  the common ratio for which the consecutive reference velocities form a geometric progression is found. The number of reference velocities  $m$  is determined by the smallest integer as follows:

$$\rho^{m-1} \geq R. \quad (2.13)$$

Therefore, we obtain:

$$m = \begin{cases} \frac{\ln R}{\ln \rho} + 1, & \text{if } \frac{\ln R}{\ln \rho} \text{ is an integer} \\ \left\lfloor \frac{\ln R}{\ln \rho} + 1 \right\rfloor + 1, & \text{if } \left\lfloor \frac{\ln R}{\ln \rho} + 1 \right\rfloor \text{ is not an integer,} \end{cases} \quad (2.14)$$

where  $\lfloor \cdot \rfloor$  denotes the integer part of the real number. Then the consecutive reference velocities are chosen as  $v_1, v_2, v_3, \dots, v_{m-1}, v_m$ , where  $v_1 = v_{\min}$  and  $v_1, v_2, v_3, \dots, v_{m-1}, v_m$ , where  $v_1 = v_{\min}$ .

Based on this we have,

$$v_{\max} \leq v_m < \rho v_{\max}. \quad (2.15)$$

## Statistical Method

This method was introduced by Bagaini [31]. Here, we take the minimum and maximum velocities from the velocity model and denote them as  $v_{\max}$  and  $v_{\min}$ , respectively. We divide the velocity range  $[v_{\max}, v_{\min}]$  into  $L$  subintervals  $[c_0, c_1), [c_1, c_2) \dots [c_{L-2}, c_{L-1}), [c_{L-1}, c_L]$  based on:

$$c_i = v_{\min} + \frac{i(v_{\max} - v_{\min})}{L}. \quad (2.16)$$

Suppose in the velocity model we have  $n_x$  lateral velocities  $v(x_l, z)$ , ( $l = 1, 2, \dots, n_x$ ), at some depth. These velocities will fall into one of the above  $L$  subintervals. Let  $n_i$  denote the number of velocities that fall into this interval  $[c_0, c_1), [c_1, c_2) \dots [c_{L-2}, c_{L-1})$  and  $n_{L-1}$  is the number of reference velocities falling into the interval  $[c_{L-1}, c_L]$ .

Let  $P_i$  denote probability density at each bin and the sum of probability is equal to 1.  $P_i = \frac{n_i}{n_x}, i = 0, 1, 2, \dots, L - 1$ . Note that  $0 \leq P_i \leq 1$  and  $\sum_{i=0}^{L-1} P_i = 1$ . Then we construct a number:

$$B = \exp \left[ \sum_{P_i \neq 0} \ln P_i^{-P_i} \right] = \prod_{P_i \neq 0} P_i^{-P_i} \quad (2.17)$$

.

Using the Hardy, Littlewood and Poylas inequality it can be shown that :

$$1 \leq B \leq L. \quad (2.18)$$

Finally the number of reference velocities can be chosen as

$$m = B + [0.5] + 1, \quad (2.19)$$

Where  $[.]$  denotes the integer part of the real number. Therefore, using the



above inequality we have:

$$2 \leq m \leq L + 1. \quad (2.20)$$

Now to determine the reference velocities we use  $Y_0 = 0$  and  $Y_j = \sum_{i=0}^{j-1} P_i, j = 1, 2, 3, \dots, L$ . We then set  $v_0 = v_{\min}$  if there exist any  $j$  such that  $Y_j < \frac{i}{m-1} \leq Y_{j+1}$ , then the reference velocities can be determined as follows:

$$v_i = c_j + \frac{\frac{i}{m-1} - Y_j}{Y_{j+1} - Y_j} (c_{j+1} - c_j), i = 1, 2, \dots, m - 1. \quad (2.21)$$

Then we have the  $m$  reference velocities

$$v_0, v_1, v_2, \dots, v_{m-1}.$$

### 2.6.3 Simulation Results

The stacked 3D SEG/EAGE salt model data set is migrated using 3D Rectangular PSPI for a depth step  $\Delta z = 20$  m, in-line and cross-line intervals  $\Delta x = \Delta y = 40$  m, time sampling interval  $\Delta t = 0.008$  s,  $f = 50$  Hz. Figures 2.10 – 2.11 show two cross-line slices of migrated sections. Also, two slices of the in-line section are shown in Figures 2.12 – 2.13. Depth slices are shown in Figures 2.14 – 2.15.

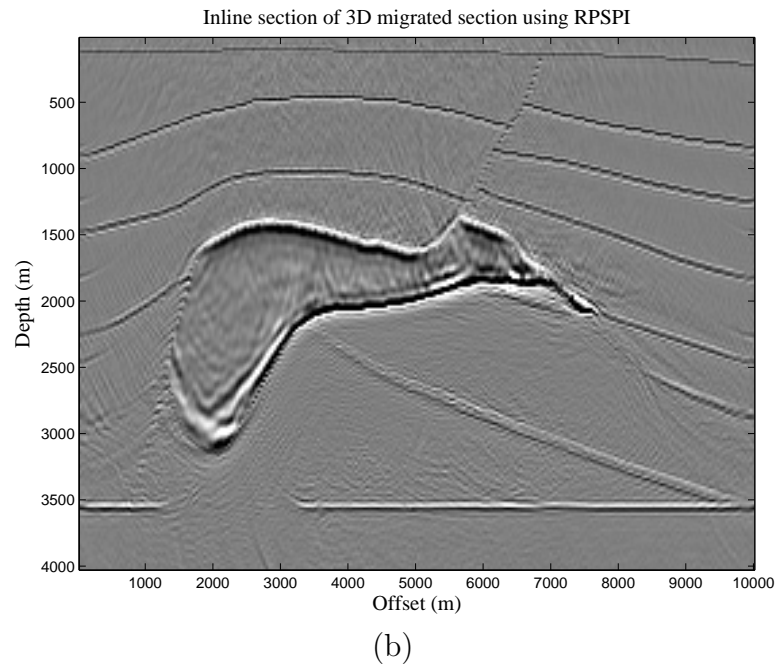
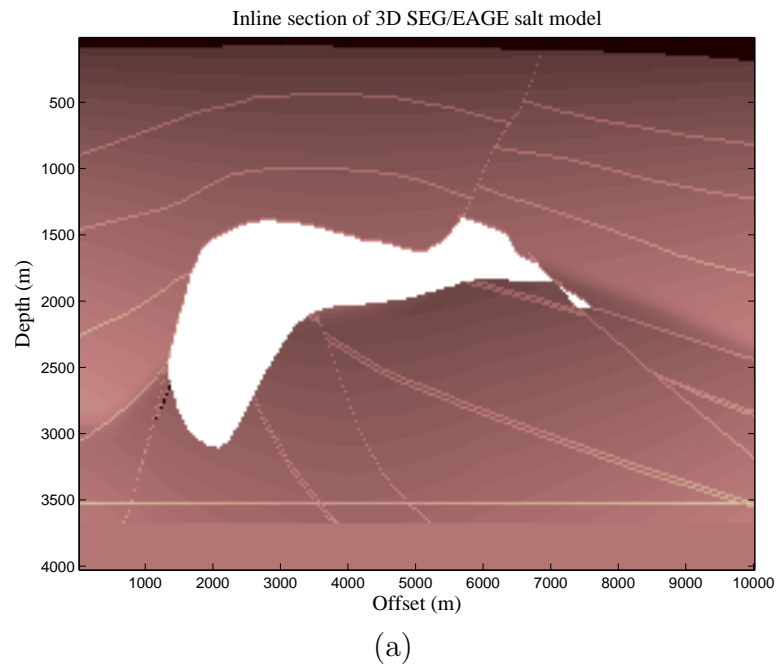


Figure 2.9: Inline section (69) of (a) SEG/EAGE salt model, (b) Migration result using rectangular phase shift plus interpolation.

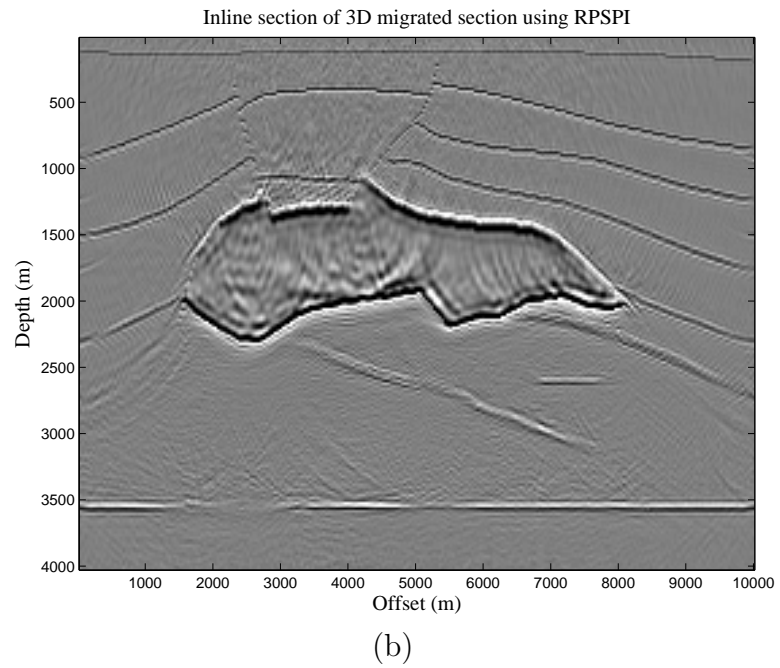
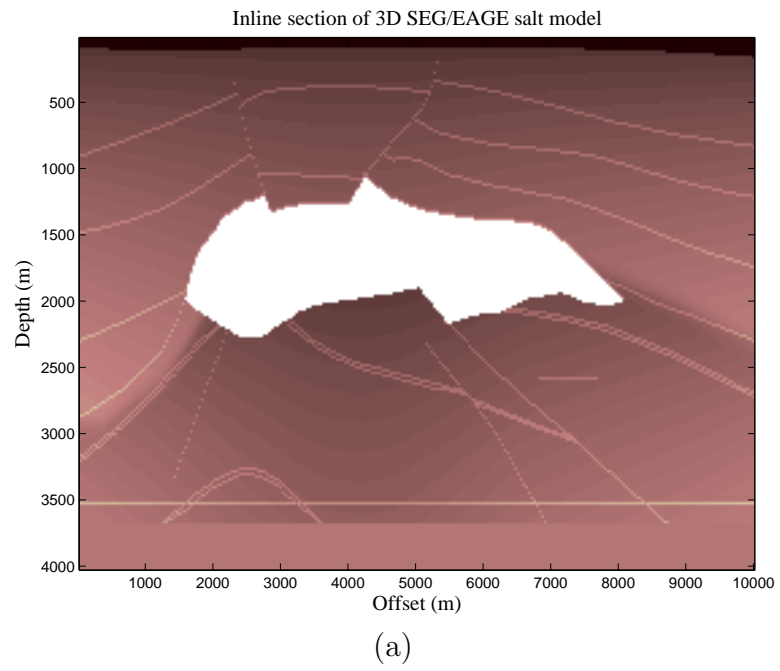


Figure 2.10: Inline section (99) of (a) SEG/EAGE salt model, (b) Migration result using rectangular phase shift plus interpolation.

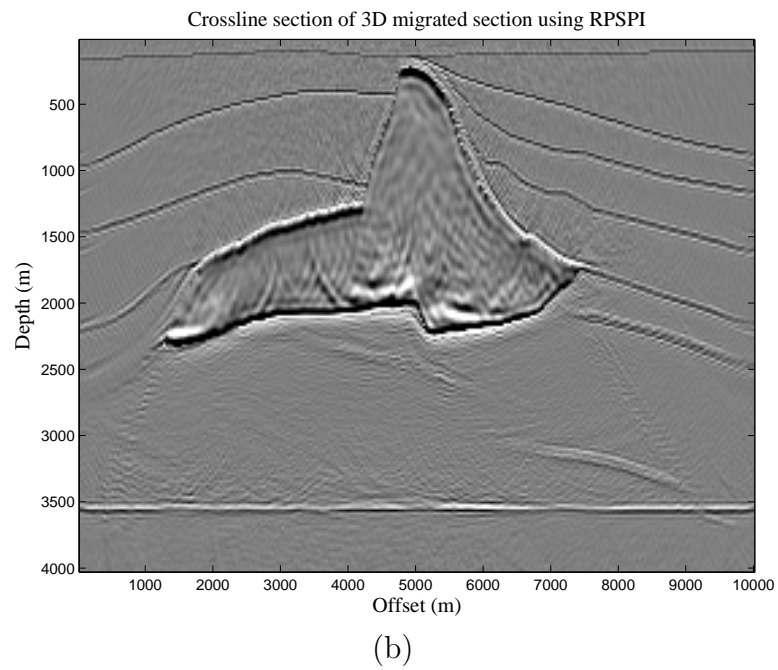
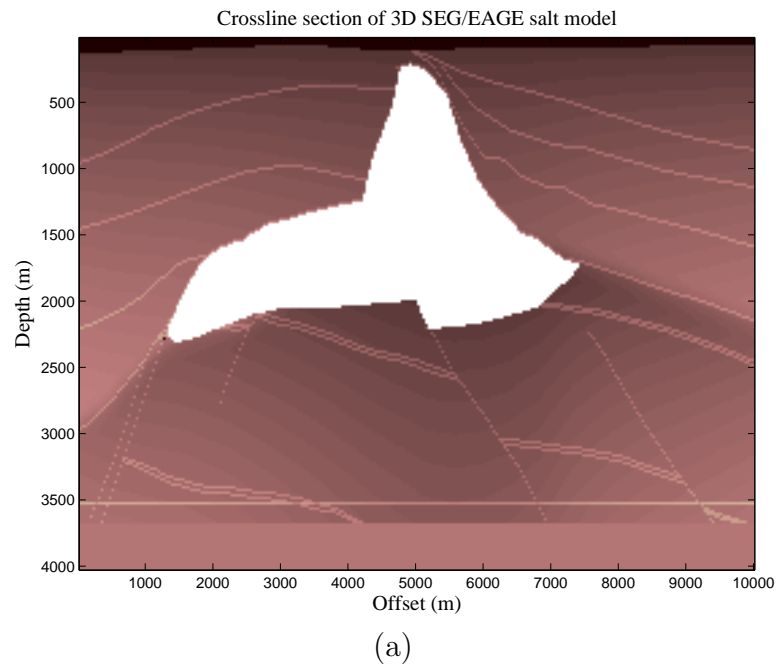


Figure 2.11: Crossline section (87) of (a) SEG/EAGE salt model, (b) Migration result using rectangular phase shift plus interpolation.

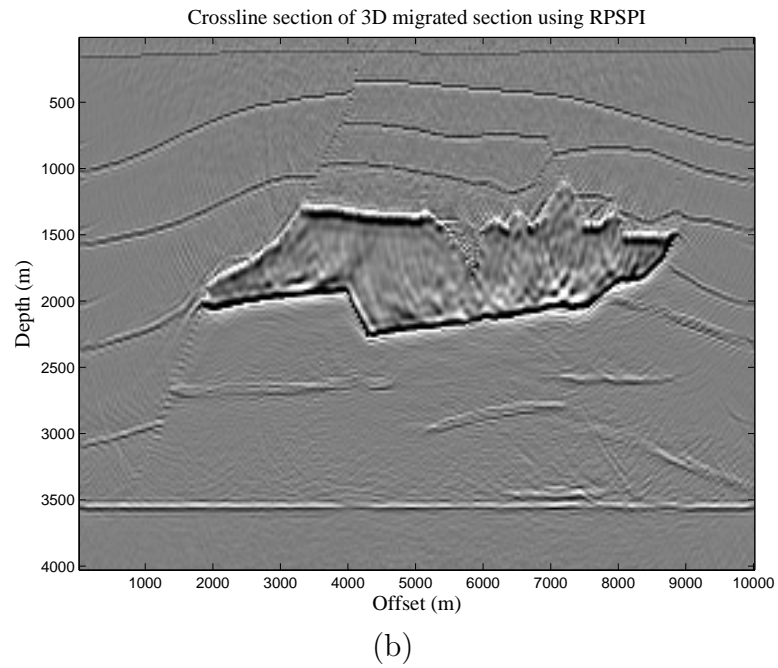
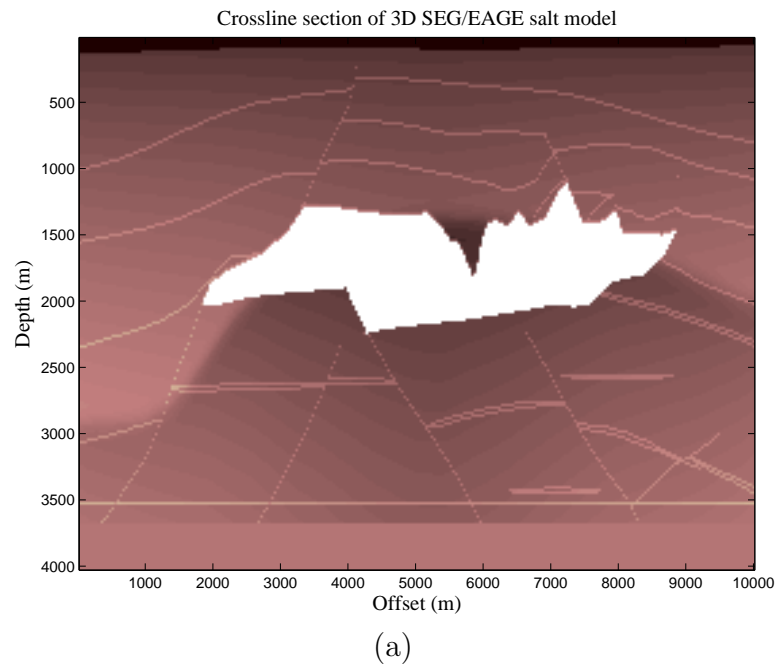


Figure 2.12: Crossline section (126) of (a) SEG/EAGE salt model, (b) Migration result using rectangular phase shift plus interpolation.

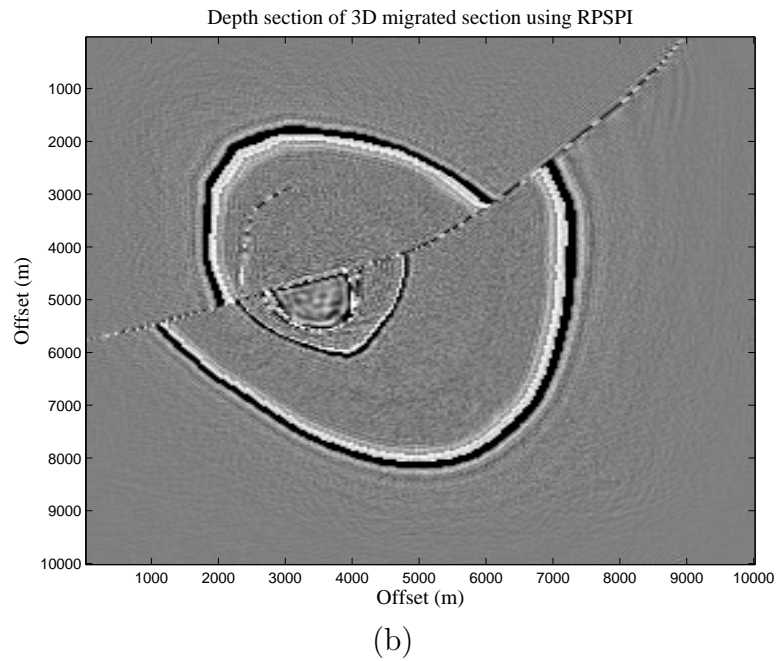
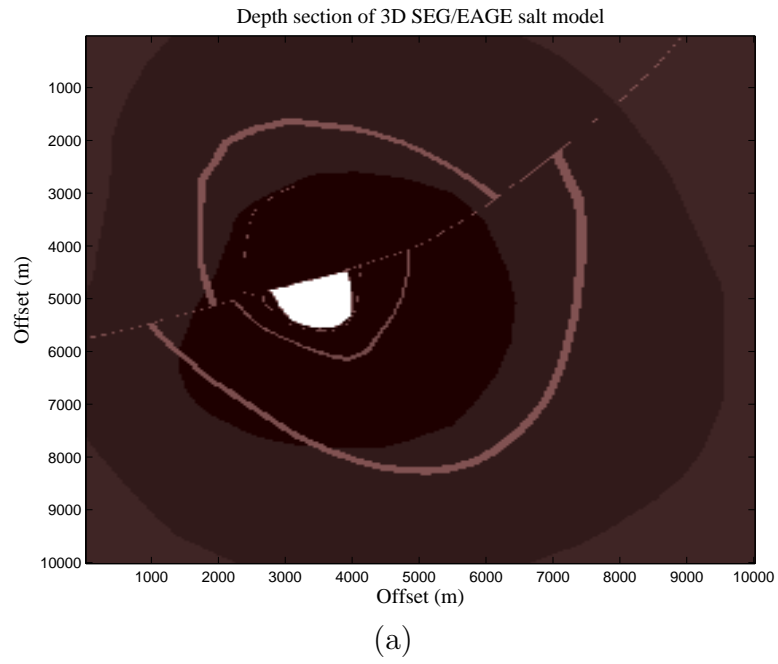


Figure 2.13: Depth section (29) of (a) SEG/EAGE salt model, (b) Migration result using rectangular phase shift plus interpolation.

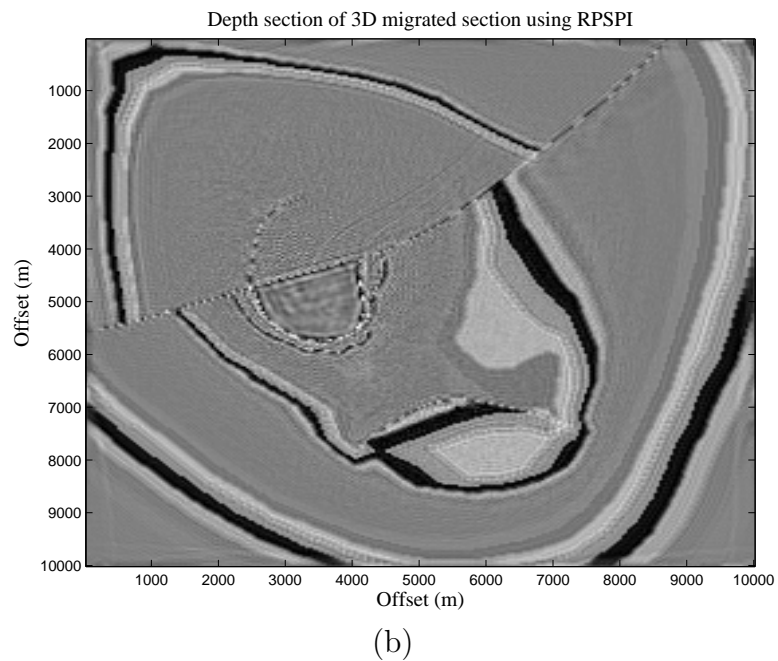
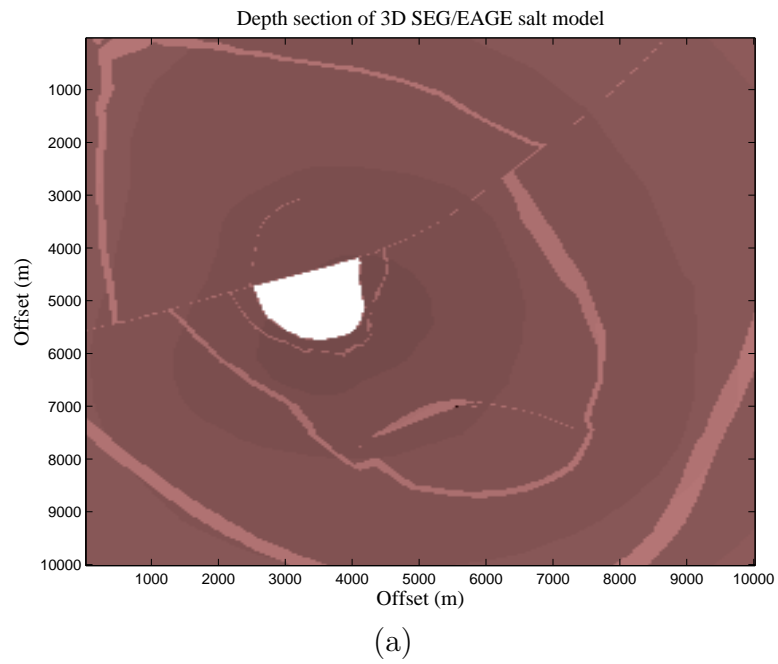


Figure 2.14: Depth section (43) of (a) SEG/EAGE salt model, (b) Migration result using rectangular phase shift plus interpolation.

## 2.7 Hexagonal Data processing

Two dimensional spatial signal sampling can be considered as tiling of Euclidean plane. Sampling can be achieved by dividing the Euclidean plane into regular and reproducible tiles, then analyzing the signal in each tile [4]. If all the tiles have same shape and size then its called monohedral tiling. Only three monohedral tilings are possible as shown in Figure 2.15.

From Figure 2.17, it is evident that for circularly band-limited signals hexagonal sampling is the more efficient than rectangular, as hexagon is better approximation to a circle [6]. Further, among the three monohedral tiling schemes, hexagonal scheme has higher sampling efficiency as shown in Table 2.1.

The mean sampling density in the spatial domain is less for hexagonal sampling. Generally, it can be shown that mean sampling density is proportional to the area of the assumed band shape [5]. The mean sampling density for the rectangular approach is greater in the spatial domain than for the hexagonal case. Thereby, for a circularly band limited signals, hexagonal sampling uses 13.4% fewer samples than rectangular [15].

Bardan [6] showed that the frequency-wavenumber ( $f - k_x - k_y$ ) response of a 3-D seismic data set can be approximated by a domain bounded by two cones i.e. for each frequency slice, the 2-D wavenumber spectra are circularly band limited



as shown in Figure 2.18. Thus, hexagonal sampling is the ideal for seismic data acquisition.

### 2.7.1 Hexagonal Data Handling

Many approaches were proposed to deal with the hexagonal data, most of them were based on the rectangular sampling. One method proposed was to shift alternate rows by half the pixel distance, the result is like a brick wall. Overington [4] observed that hexagonal lattice can be approximated by a brick wall of rectangle with  $8 \times 7$  aspect ratio. Laine [32] followed the quincunx sampling with linear interpolation to double the size in the horizontal direction and triple in the vertical direction, to emphasize the hexagonal arrangement. A better scheme to address hexagonal grids would be to use coordinate axes along the axes of symmetry of hexagon, Her [33] proposed approximation using three coordinate axes scheme where the axes were  $120^\circ$  apart. Burt [34] proposed the  $B_h$  coordinate axes scheme with two non-orthogonal axes at  $120^\circ$  apart as shown in Figure 2.21, all these methods were inefficient in processing data.

Sheridan introduced Spiral Architecture (SA) for hexagonal data indexing [16, 4], which uses base-7 indexing i.e. indexes go from 0 to 6 and then 10 to 66, as shown in Figure 3.1. It is described in more detail in the Section 3.3. For further details readers are encouraged to read [4].

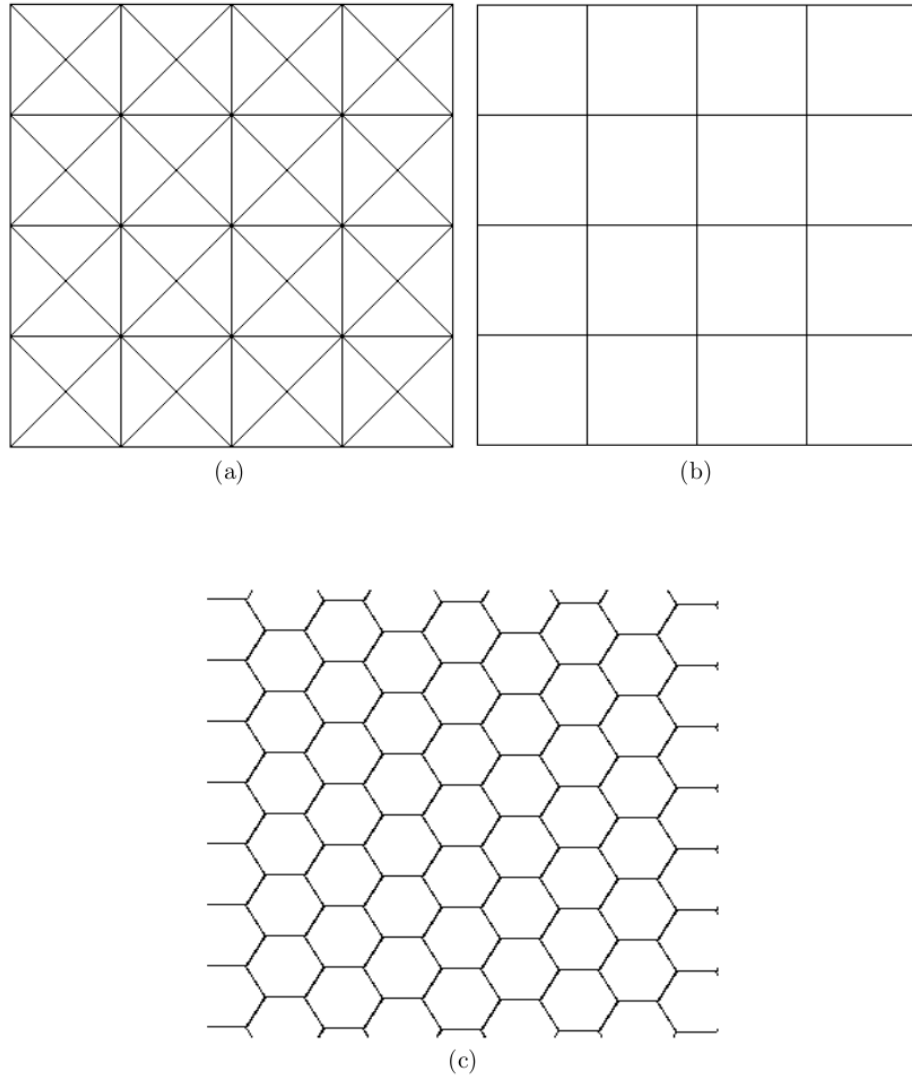
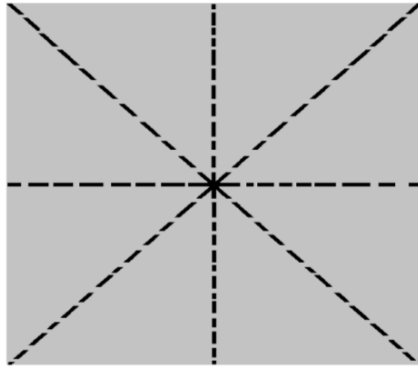


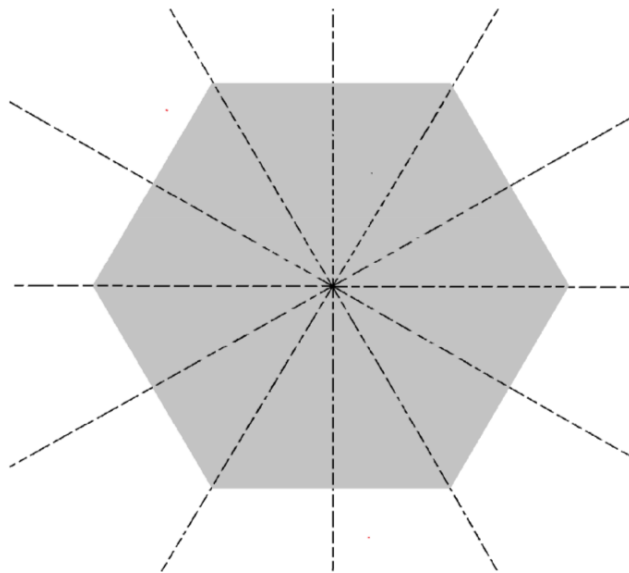
Figure 2.15: Types of monohedral tiling (a) triangular, (b) rectangular and (c) hexagonal, covering the Euclidean plane regularly without gaps.

Tessellation	Sampling Efficiency
Triangular	$\leq 60.46\%$
Rectangular	$\leq 78.56\%$
Hexagonal	$90.69\%$

Table 2.1: Sampling efficiency comparison for the three monohedral tiling.



(a)



(b)

Figure 2.16: (a) square with 8 folds of symmetry, (b) hexagon with 12 folds of symmetry (courtesy of [4]).

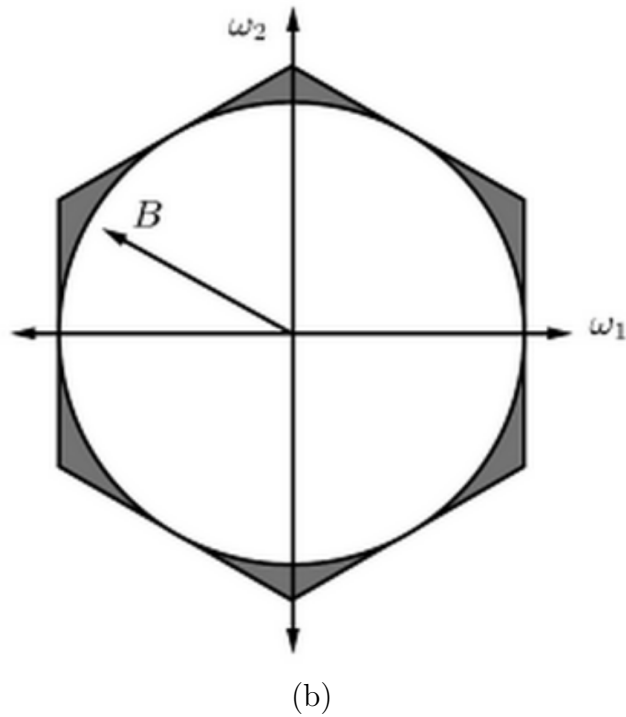
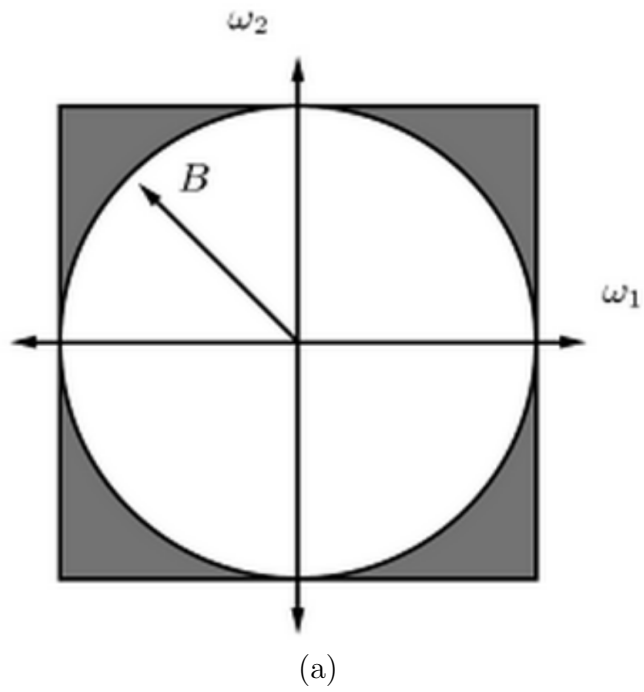


Figure 2.17: a circularly band limited signal inscribed in (a) square and (b) hexagon. Inaccurate representation of circle is 27.3% and 10.2% by square and hexagon respectively. (courtesy of [5]).

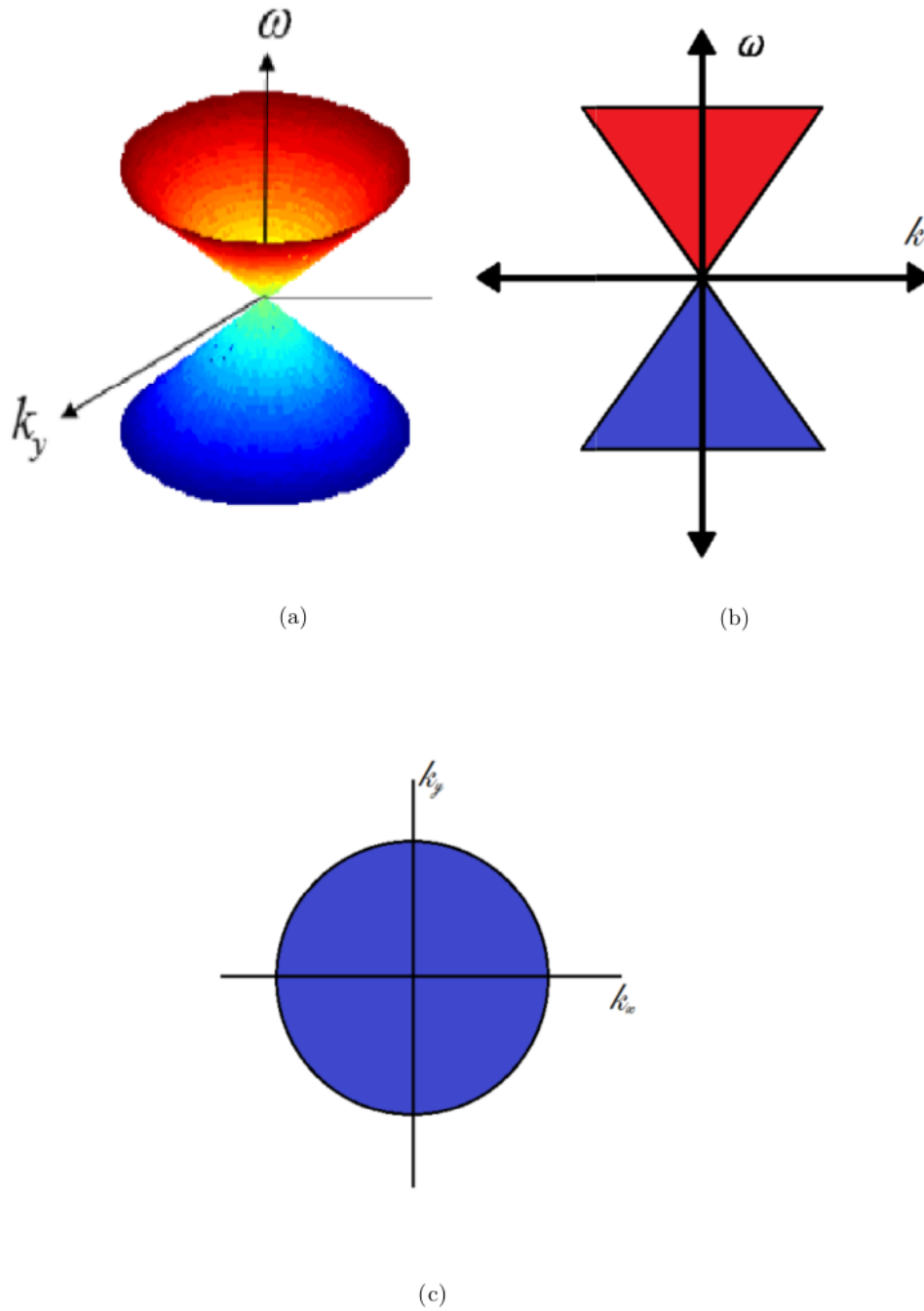
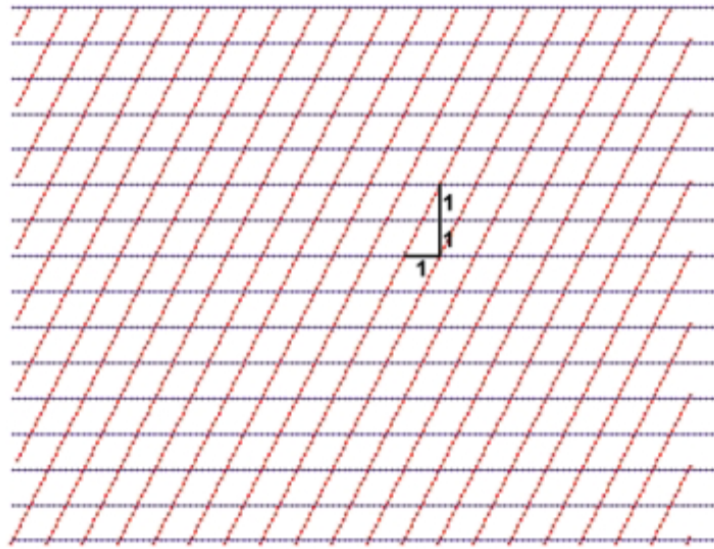
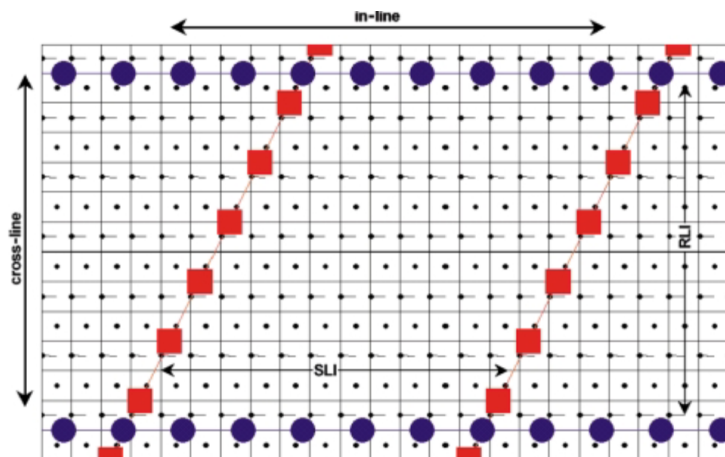


Figure 2.18: Seismic band region (a) In the  $k_x - k_y - \omega$  space, (b) In the  $k - \omega$  plane and (c) in the  $k_x - k_y$  plane (courtesy of [6]).



(a)



(b)

Figure 2.19: Shows (a) hexagonal acquisition layout using rectangular bins, (b) zoomed layout. The shot locations are represented by squares and receiver by circles (courtesy of [1]).

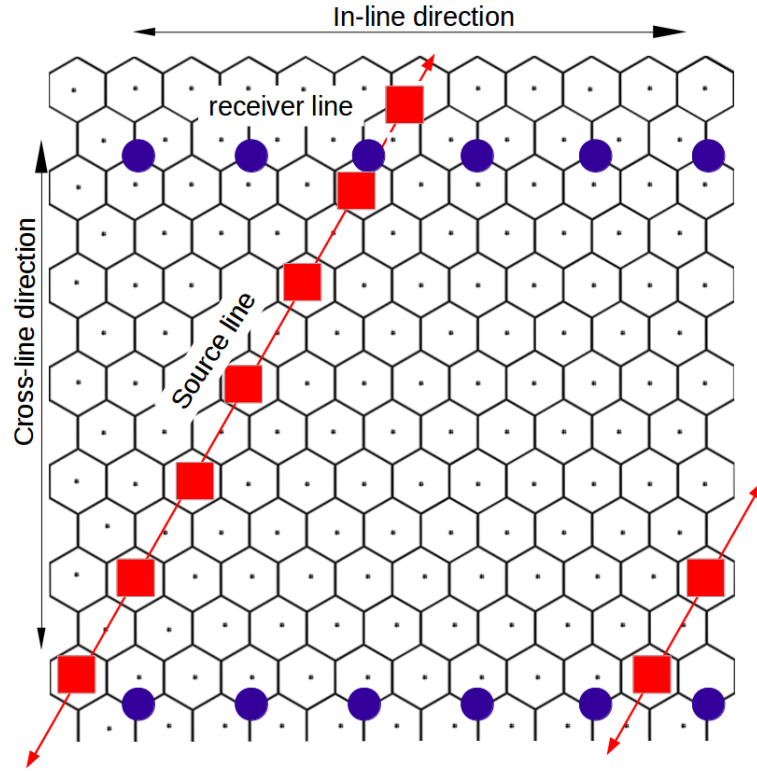


Figure 2.20: Hexagonal acquisition layout using hexagonal bins (courtesy of [6]).

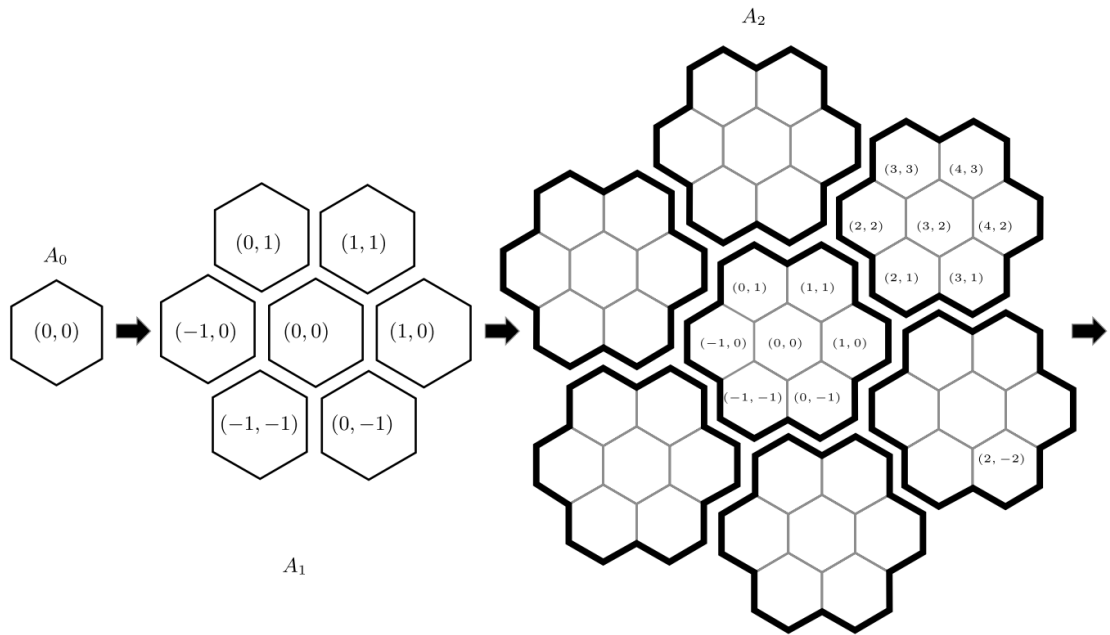


Figure 2.21: Hexagonal indexing in the  $B_h$  coordinate system for aggregate level 0, 1 and 2 (courtesy of [4]).



## 2.8 Summary

This chapter describes the flow of seismic migration process, starting from the acquisition geometry to processing/imaging. The 3D PSPI imaging technique is developed and the 3D SEG/EAGE salt model data set is migrated and results are shown. The PSPI imaging technique though yields better quality of images requires higher computation resources. The chapter also describes that the hexagonal seismic acquisition is better choice than the conventional approach. This will be illustrated in the next chapter.

## CHAPTER 3

# HEXAGONAL PHASE SHIFT PLUS INTERPOLATION WITH HEXAGONALLY SAMPLED DATA

### 3.1 Introduction

The 3D seismic acquisition techniques were not very popular until the 1970's due to the computation complexity involved in processing of the 3D data. With the advent of modern computing capabilities 3D seismic data acquisition has become an economical solution [1], reducing the exploration risks. The information and accuracy of 3D seismic imaging has catapulted the industry to switch from 2D to 3D seismic data acquisition [2]. The demand for higher resolution of seismic

data has also seen a substantial increase in the past four decades [14], employing large number of receiver channels, the data so acquired is enormous and requires optimal processing techniques to be used.

One-way wave equation migration (OWE) techniques have been very popular for their easy of computational complexity [35]. One of the OWE techniques is the phase shift plus interpolation (PSPI) migration introduced by [24], it is very accurate and can account for the lateral velocity variations, when sufficient number of reference velocities are used. Bagaini [36] proposed a statistical method for selection of optimal number of reference velocities.

The migration techniques have mostly been used in the grids where the in-line and cross-line directions are designed as orthogonal. However, researchers have developed migration techniques for the non-orthogonal sampling grids in the past because of their higher sampling and computational efficiency [37, 6, 38, 39, 40]. Hexagonal grid sampling is one of the very widely used non-orthogonal techniques. It has been proved to be 13.4% more efficient than the rectangular sampling in 2D by Mersereau [15]. Bardan showed that the frequency-wavenumber ( $f - k_x - k_y$ ) response of a 3-D seismic data set can be approximated by a domain bounded by two cones i.e. for each frequency slice, the 2-D wavenumber spectra are circularly band limited [6]. The optimal sampling technique for circularly band limited signals is the hexagonal grid [15]. Thus, an ideal scheme for sampling seismic

data is by using hexagonal grids [6, 41]. In this chapter, we use the 3D PSPI imaging for its accuracy, along with statistical method for reference velocities selection, to migrate 3D hexagonally sampled data using spiral architecture. We show that it is more efficient than the rectangular counterpart.

## 3.2 Spiral Architecture (SA)

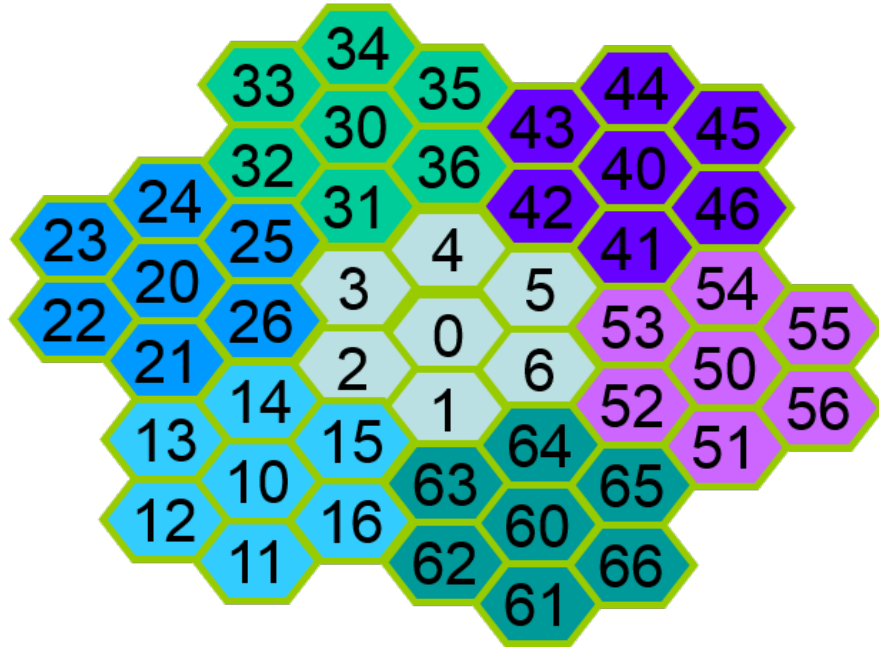
In the work carried out by [42, 10, 6, 41, 43, 44, 45] attempts were made to process hexagonal seismic data. Since in-line and cross-line axes are not orthogonal, it was difficult to give each hexagonal sample a location and thus a semi-hexagonal process was proposed to handle the location of samples [32, 33].

Researchers in the field of image processing and computer vision proposed various indexing schemes for the hexagonal grids [4, 46, 47, 48, 49, 50, 16] from zero insertion between samples, to interpolating alternate rows to produce shifted rows forming a hexagon [32], in the process doubling the amount of data which is undesirable, moreover the wavenumber response of the filters will be aliased due to zero insertion. Others proposed that better choice of axes is along the axes of symmetry of the hexagon [51, 52, 33], all these methods were inefficient in processing data.

Sheridan introduced Spiral Architecture (SA) for hexagonal data indexing

[16, 4]. The SA uses base-7 indexing. The indexes go from 0 to 6 and then 10 to 66. The indexing starts with 0 at the center instead of a corner in the rectangular scheme. The hexagonal grid with 0 index is called as aggregate level '0', surrounded by index 1 to 6, which forms aggregate level '1', with 7 elements. The aggregate level '2' is formed by repeating the level '1' aggregate six times around it and would have  $7^2$  samples, as shown in Figure 3.1.

A major benefit of SA is that 2D data can be stored and processed as 1D data based on the 1D addresses. This is illustrated as the 2D data in Figure 3.1 (a) is stored in SA as 1D vector shown in Figure 3.1 (b). This means that a 2D operations on data, like convolution, fourier transform would now become 1D, thus the processing would be much more efficient in time. Furthermore, because of the 12 fold symmetry exhibited by the hexagonal structure against the 8 fold symmetry of rectangle, it can represent a curvature much more efficiently than a rectangular structure, producing better results for seismic interpreters.

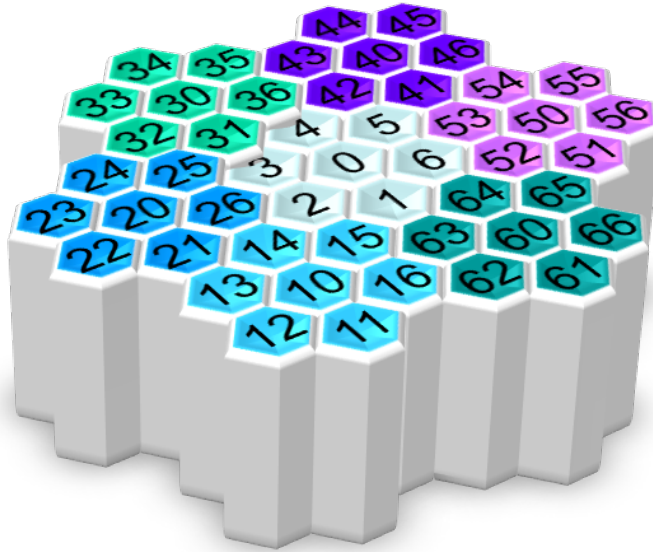


(a)

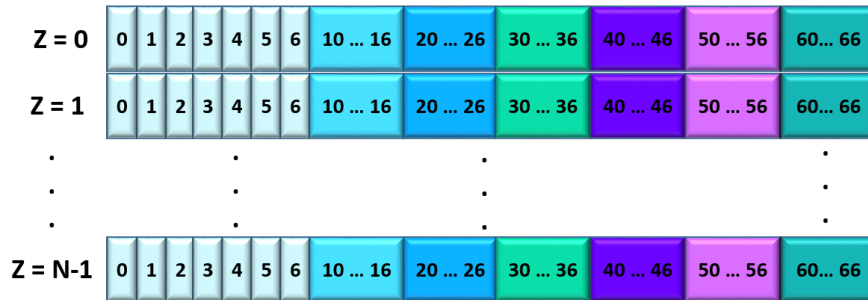


(b)

Figure 3.1: (a) 2D data representation in spiral architecture, (b) stored as 1D vector (courtesy of [7]).



(a)



(b)

Figure 3.2: (a) 3D data representation in spiral architecture, (b) stored as 2D array (Modified after [7]).

### 3.3 3D Hexagonal Phase Shift Plus Interpolation (HPSPI) in SA

PSPI is a migration method that can deal with strong lateral velocity variations [24]. Several reference velocities are used in each extrapolation step to account for the lateral velocity variation and obtain the multi-reference wavefields in the f-k domain. The final image is obtained by interpolating the reference wavefields in the frequency-space domain. We start with the PSPI equations in rectangular domain proposed by [24]:

$$P_0(x, y, z, \omega) = P(x, y, z, \omega) e^{i\frac{\omega}{v(x,y,z)}}, \quad (3.1)$$

and

$$P^*(k_x, k_y, z + dz, \omega) = P_0(k_x, k_y, z, \omega) e^{i(k_z - \frac{\omega}{v_{ref}})dz}, \quad (3.2)$$

where

$$k_z = \sqrt{\left(\frac{\omega}{v_{ref}}\right)^2 - (k_x^2 + k_y^2)}. \quad (3.3)$$

Equation 3.2 defines the wave extrapolation for next depth in PSPI. The 3D data set and velocity model is represented in spiral architecture as 2D matrix as shown in Figure 3.2, where the  $sp$  represents the spiral dimension and  $t$  or  $z$  represents the rectangular dimension. It should be noted that the data is spiral only in first dimension of the 2D data.



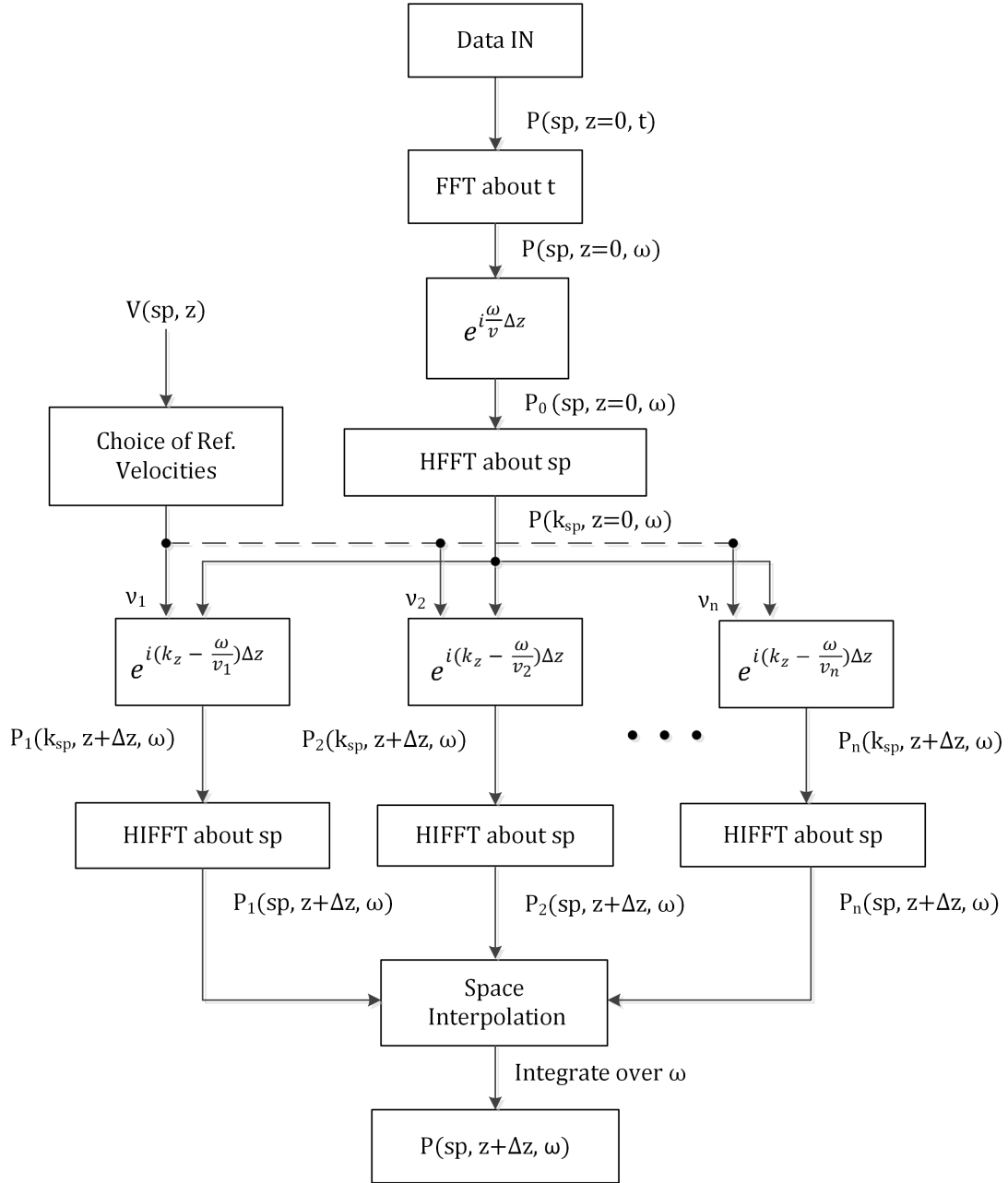


Figure 3.3: Flow chart of Hexagonal Phase Shift Plus Interpolation.

As shown in Figure 3.3, the hexagonal data in time  $t$  is converted to frequency domain using the rectangular FFT. Initial phase shift is applied to account for lateral velocity variations [24] and then Hexagonal Fast Fourier Transform (HFFT) is applied [4] to the spiral data, to get into the  $f - k$  domain. Second time phase shift is applied, followed by Hexagonal Inverse Fast Fourier Transform (HIFFT) and interpolation to obtain the extrapolation for the next depth.

The Equations 3.1–3.3, can be rewritten for the hexagonal data as,

$$P_0(sp, z, \omega) = P(sp, z, \omega) e^{i\frac{\omega}{v(sp,z)}}, \quad (3.4)$$

$$P(k_{sp}, z + dz, \omega) = P_0(k_{sp}, z, \omega) e^{i(k_z - \frac{\omega}{v_{ref}})dz}, \quad (3.5)$$

where

$$k_z = \sqrt{\left(\frac{\omega}{v_{ref}}\right)^2 - \left(k_x^2 + k_y^2 \left(\frac{\Delta x}{\Delta y}\right)^2\right)}. \quad (3.6)$$

In Equation 3.6, the additional term  $\frac{\Delta x}{\Delta y}$  is added as the  $\Delta x \neq \Delta y$ , i.e., the cross-line interval is not equal to in-line interval in hexagonal sampling, [53, 54].

Note that the choice of reference velocities is very crucial for the PSPI accuracy. We have used Bagaini's statistical method for reference velocity selection, which has been explained in Chapter 2. The hexagonally sampled velocity model at a given depth would be a vector. Thus, the statistical method is effective in determining the reference velocities.

## 3.4 The Computational Complexity of HPSPI in SA

The computational cost of imaging with HPSPI using  $N$ -point Hexagonal Fast Fourier Transform ( $N_{HFFT}$ ) and  $n$  reference velocities ( $n_{ref}$ ) at each depth slice can be computed in the similar lines as that of [4, 8, 24]. For complex multiplications:

$$HPSPI - COST_X = 2N_{HFFT} \times n_{ref} + (n_{ref} + 2) \times N_{HFFT} \log_7 N_{HFFT}, \quad (3.7)$$

while for complex additions,

$$HPSPI - COST_+ = (n_{ref} + 2) \times (N_{HFFT} - 1) \log_7 N_{HFFT}. \quad (3.8)$$

In both cases, each complex multiplication requires six flops, while each complex addition requires two flops, as given in [29].

## 3.5 Simulation Results

### 3.5.1 The 3D seismic migration synthetic experiments

The hexagonal PSPI in spiral architecture is tested by migrating a hexagonally sampled impulse cube with a Ricker wavelet of frequency 45 Hz centered at 0.512 s. The in-line and cross-line intervals are  $\Delta x = 10m$ ,  $\Delta y = 10m$  respectively.

Time step  $\Delta t = 4ms$  and constant velocity  $c = 1000m/s$ . The depth step used is  $\Delta z = 2m$ . With a maximum frequency of 50 Hz. The impulse response of the hexagonal PSPI in SA is compared with that of the rectangular PSPI as shown in Figure 3.4. The representation of the circle in the depth slice is more accurate for the hexagonal PSPI.

### 3.5.2 Application to 3D SEG/EAGE salt model

In order to test the proposed imaging technique, we use the SEG/EAGE salt model data set, as it is challenging to image. The salt body is embedded in sediments with smoothly varying velocities [55]. We have taken a subset of the 3-D model with dimensions,  $201 \times 250 \times 250$  traces in the  $z, x$  and  $y$  directions respectively. A zero-offset data is generated with 250 traces and the time record length is 4 s (500 time samples per trace).

The SEG/EAGE salt model data set is migrated using rectangular 3D PSPI. The data set is hexagonally sampled before migrating with the hexagonal 3D PSPI technique. MATLAB 2014 is used on a machine with 20 parallel CPU cores to do the task. The machine time required is shown in Table 3.1. Slices of 3D migrated section using the rectangular and hexagonal PSPI techniques are shown in Figure 3.5–3.10.

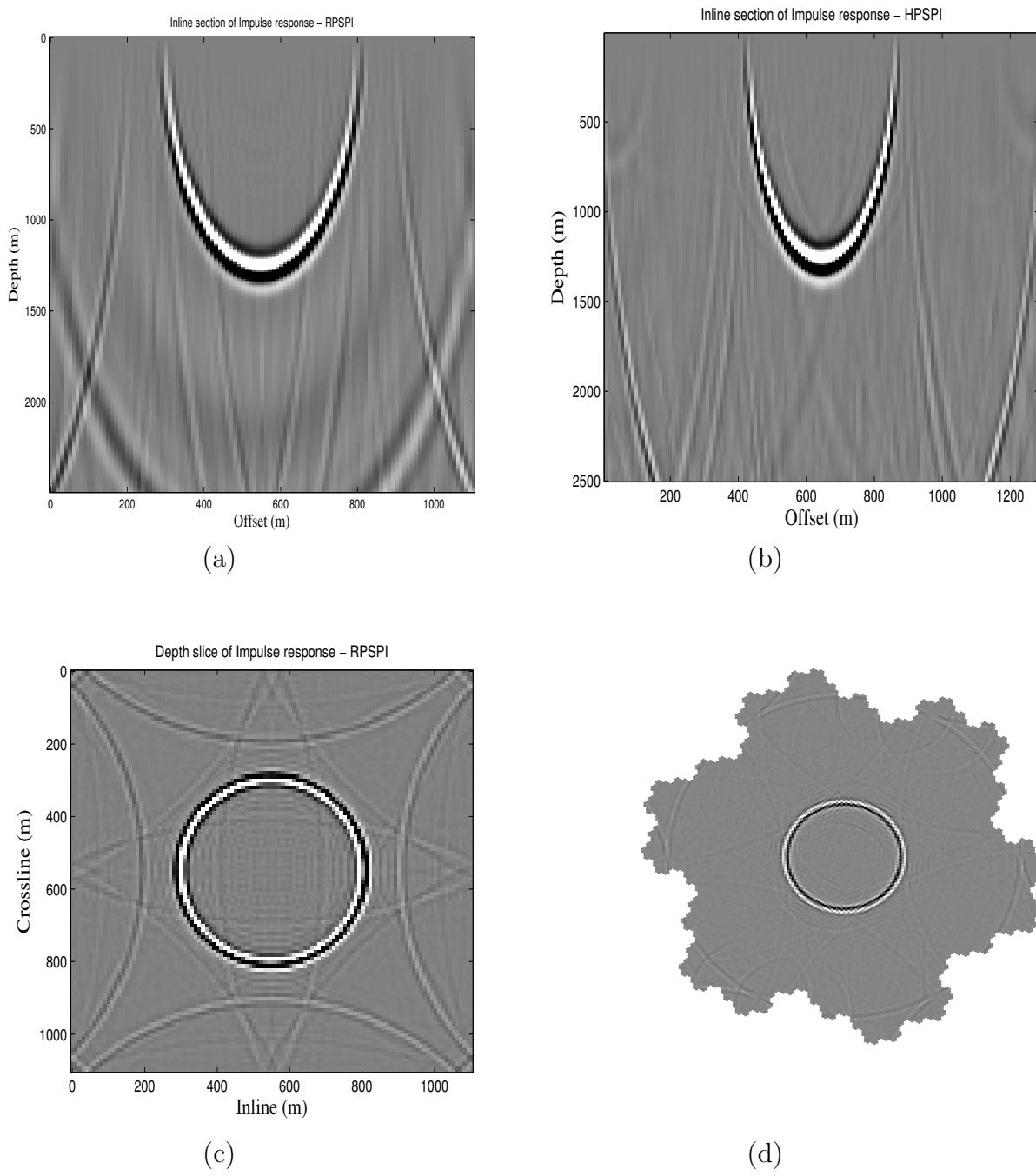


Figure 3.4: Impulse response comparison of RPSPI with HPSPI, with  $\Delta z = 2m$ ,  $\Delta x = 10m$ ,  $\Delta y = 10m$ ,  $\Delta t = 4ms$ , and  $c = 1000m/s$ . The maximum frequency is 50 Hz using (a) In-line section of impulse response migrated using rectangular PSPI, (b) In-line section of impulse response migrated using hexagonal PSPI, (c) and (d) show the depth slices of migrated image using rectangular PSPI and hexagonal PSPI respectively.

Technique	$\times$ s Flops	Savings%	Time(hrs)
Rec. PSPI	33,492,992	-	48
Hex. PSPI	14,601,462	56.4	8

Table 3.1: Comparison of number of flops (for the complex multiplications, real-complex multiplications and complex additions) at a depth slice of stacked data for migrating the 3D SEG/EAGE salt model, using rectangular and hexagonal PSPI methods (with 200 reference velocities and 2048 fourier transform points).

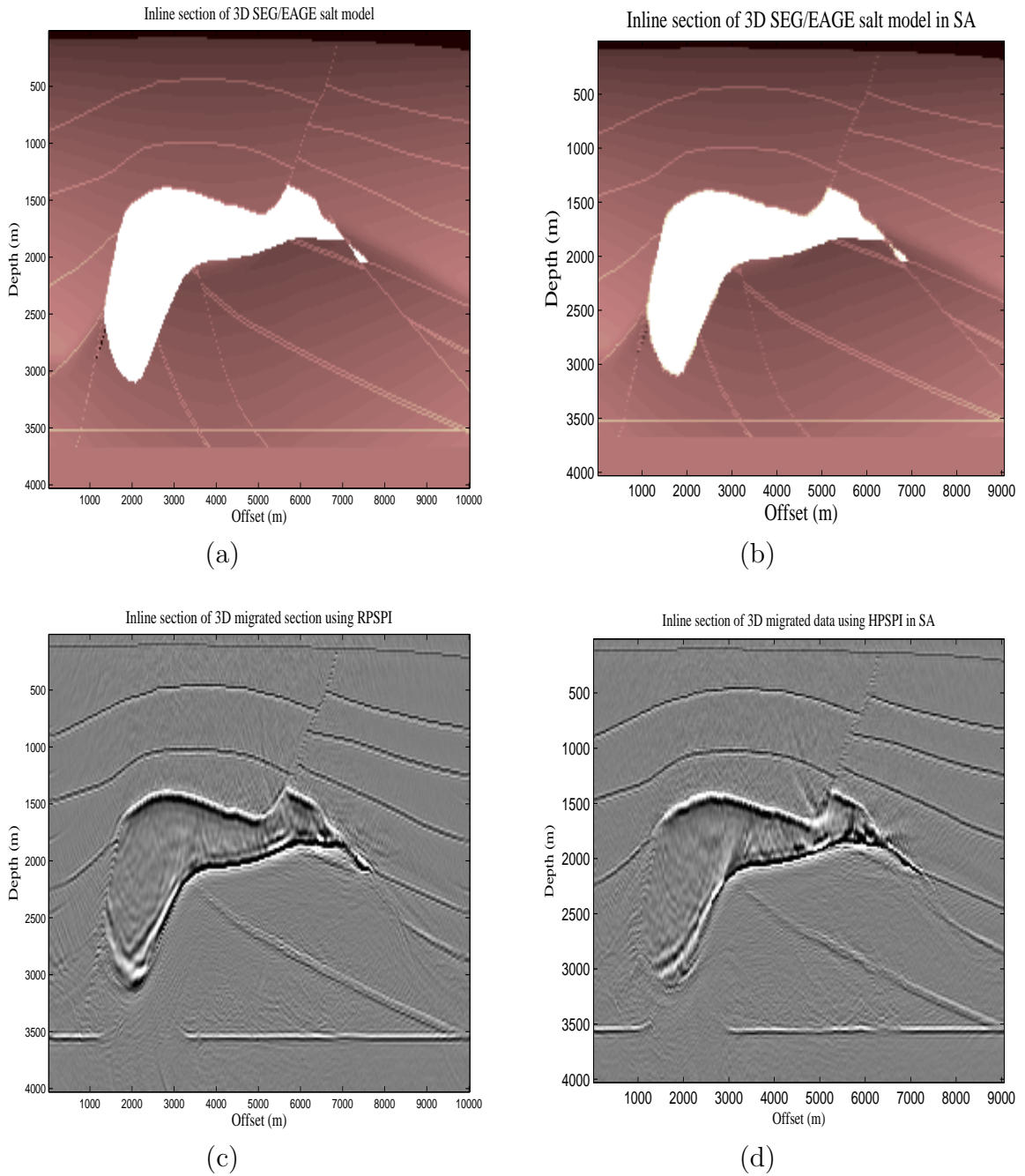


Figure 3.5: Inline section of SEG/EAGE salt model (a) original, (b) hexagonally sampled, (c) migrated section using rectangular PSPI, (d) migrated section using hexagonal PSPI in SA.

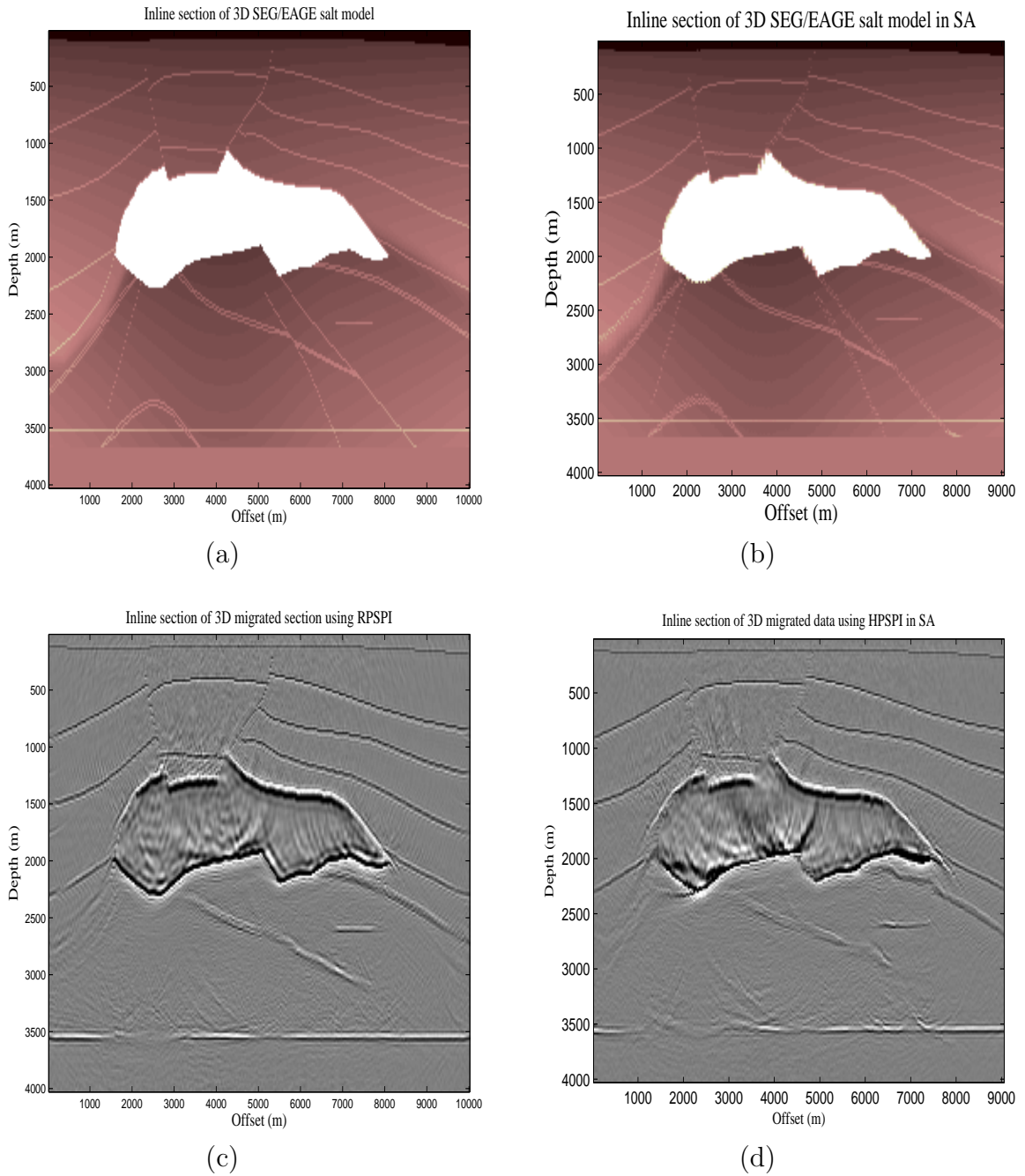


Figure 3.6: Inline section of SEG/EAGE salt model (a) original, (b) hexagonally sampled, (c) migrated section using rectangular PSPI, (d) migrated section using hexagonal PSPI in SA.



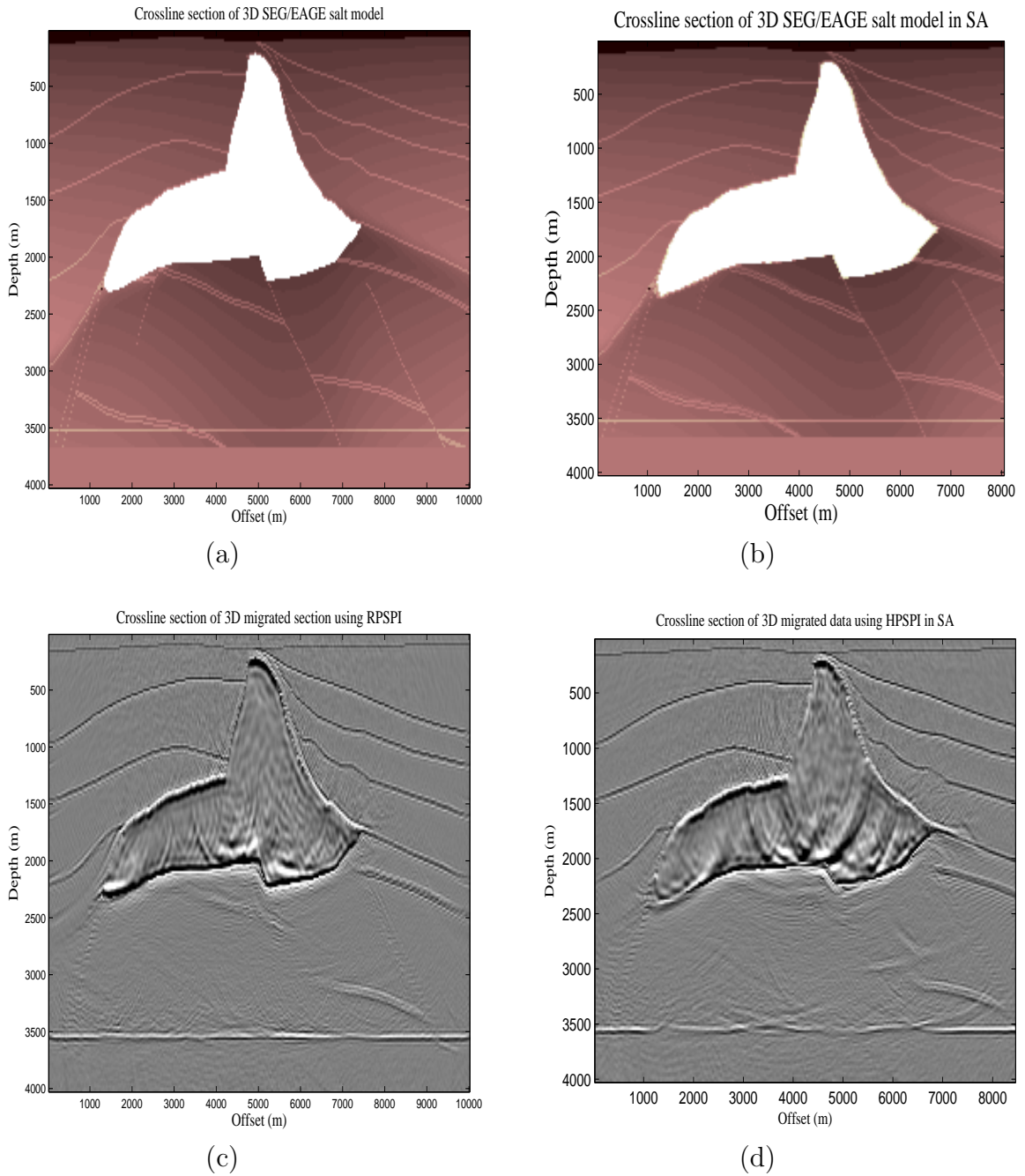


Figure 3.7: Crossline section of SEG/EAGE salt model (a) original, (b) hexagonally sampled, (c) migrated section using rectangular PSPI, (d) migrated section using hexagonal PSPI in SA.

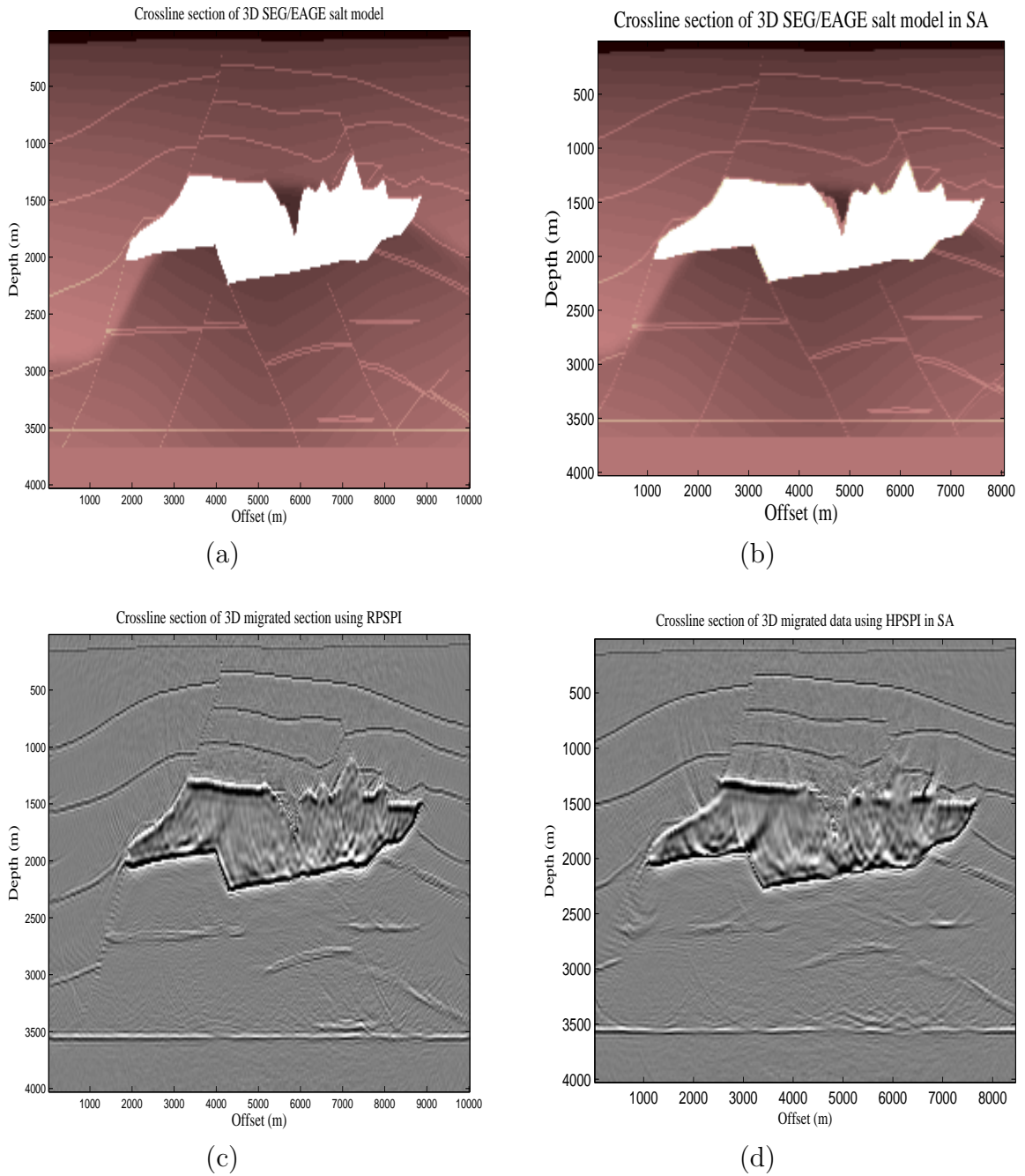
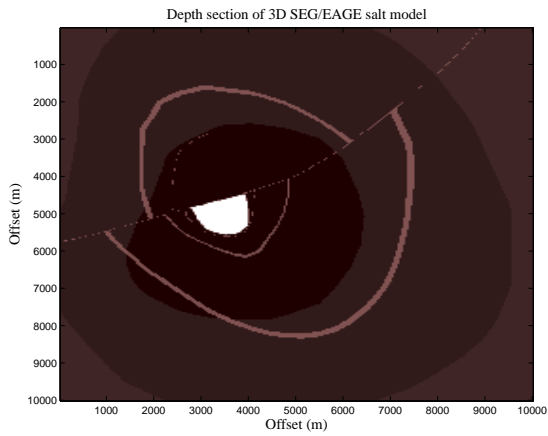
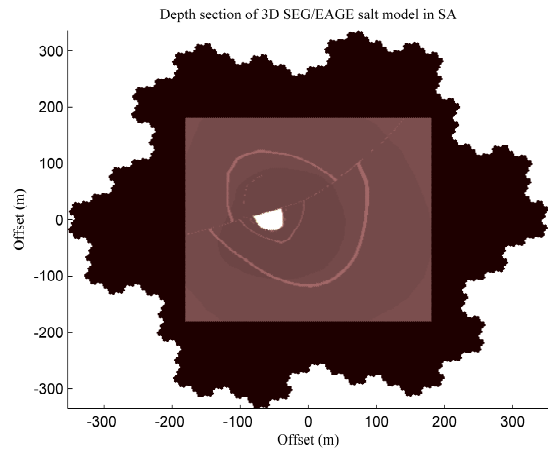


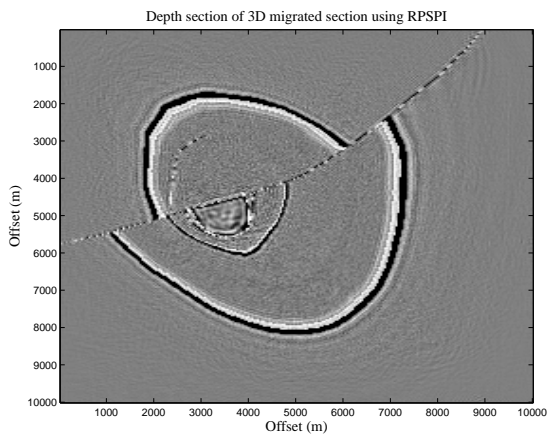
Figure 3.8: Crossline section of SEG/EAGE salt model (a) original, (b) hexagonally sampled, (c) migrated section using rectangular PSPI, (d) migrated section using hexagonal PSPI in SA.



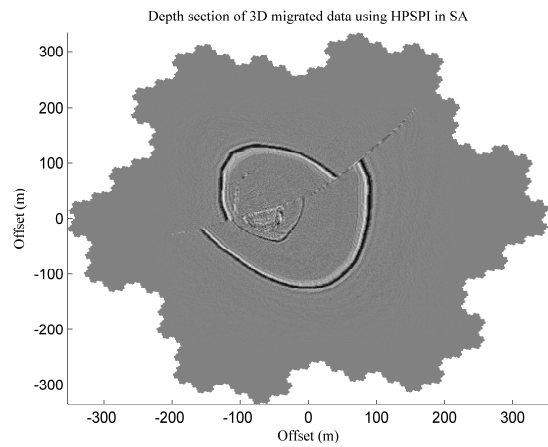
(a)



(b)

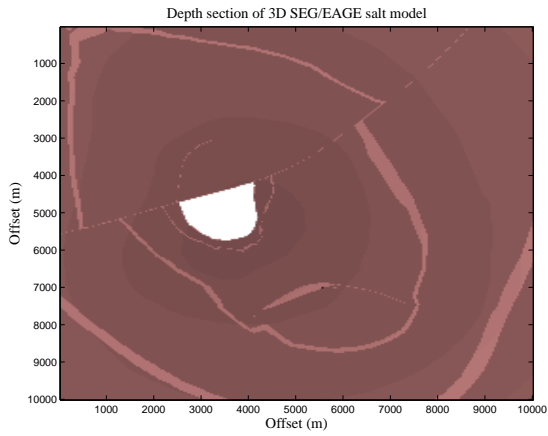


(c)

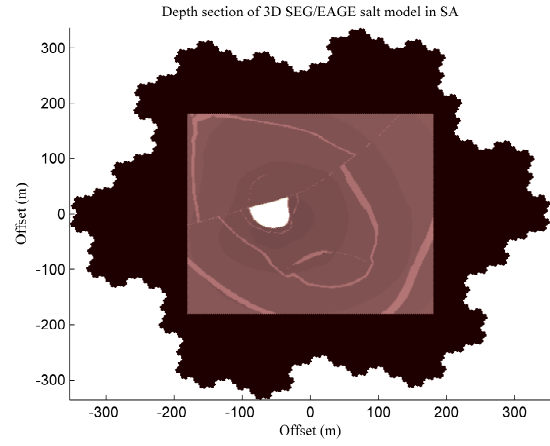


(d)

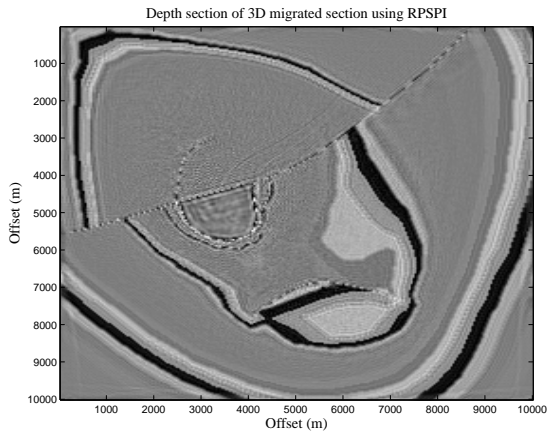
Figure 3.9: Depth section of SEG/EAGE salt model (a) original, (b) hexagonally sampled, (c) migrated section using rectangular PSPI, (d) migrated section using hexagonal PSPI in SA.



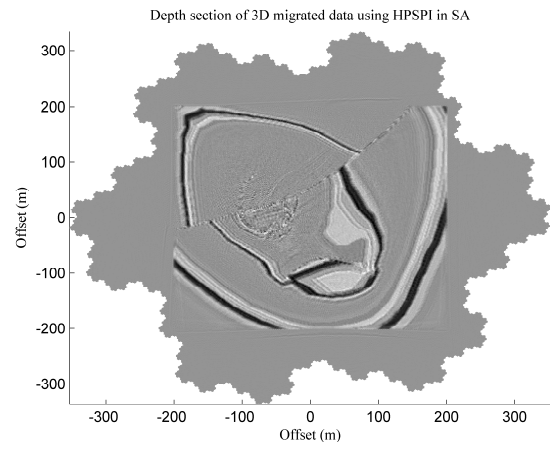
(a)



(b)



(c)



(d)

Figure 3.10: Depth section of SEG/EAGE salt model (a) original, (b) hexagonally sampled, (c) migrated section using rectangular PSPI, (d) migrated section using hexagonal PSPI in SA.

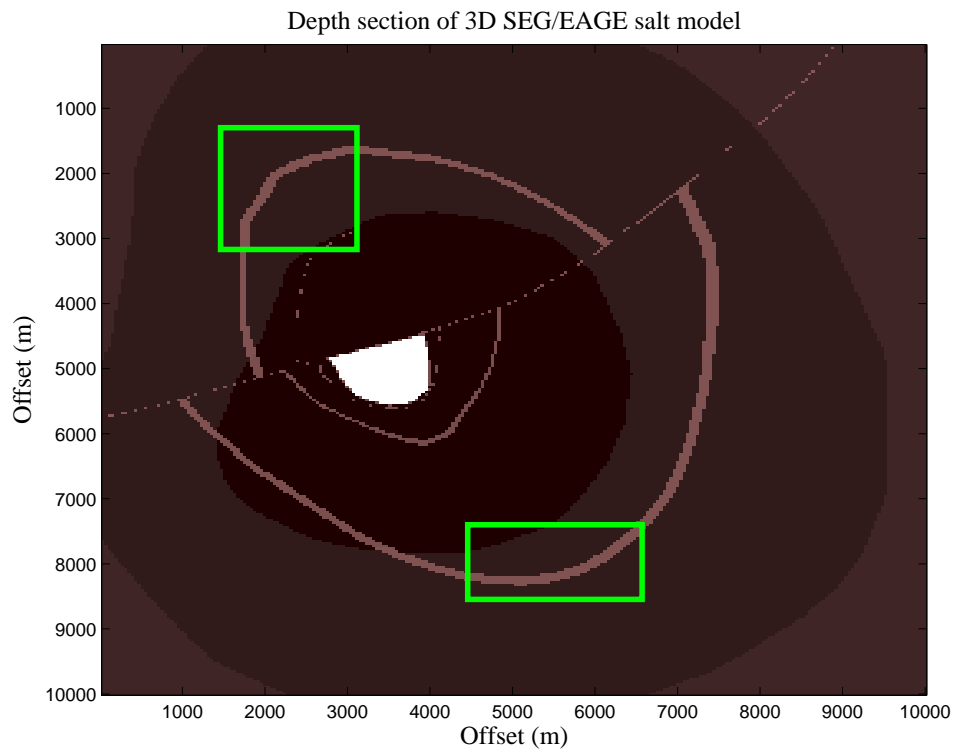


Figure 3.11: Challenging parts of the depth slice of SEG/EAGE salt model are highlighted by rectangles. The rectangle on top and bottom will be referred as box-1 and box-2 respectively.

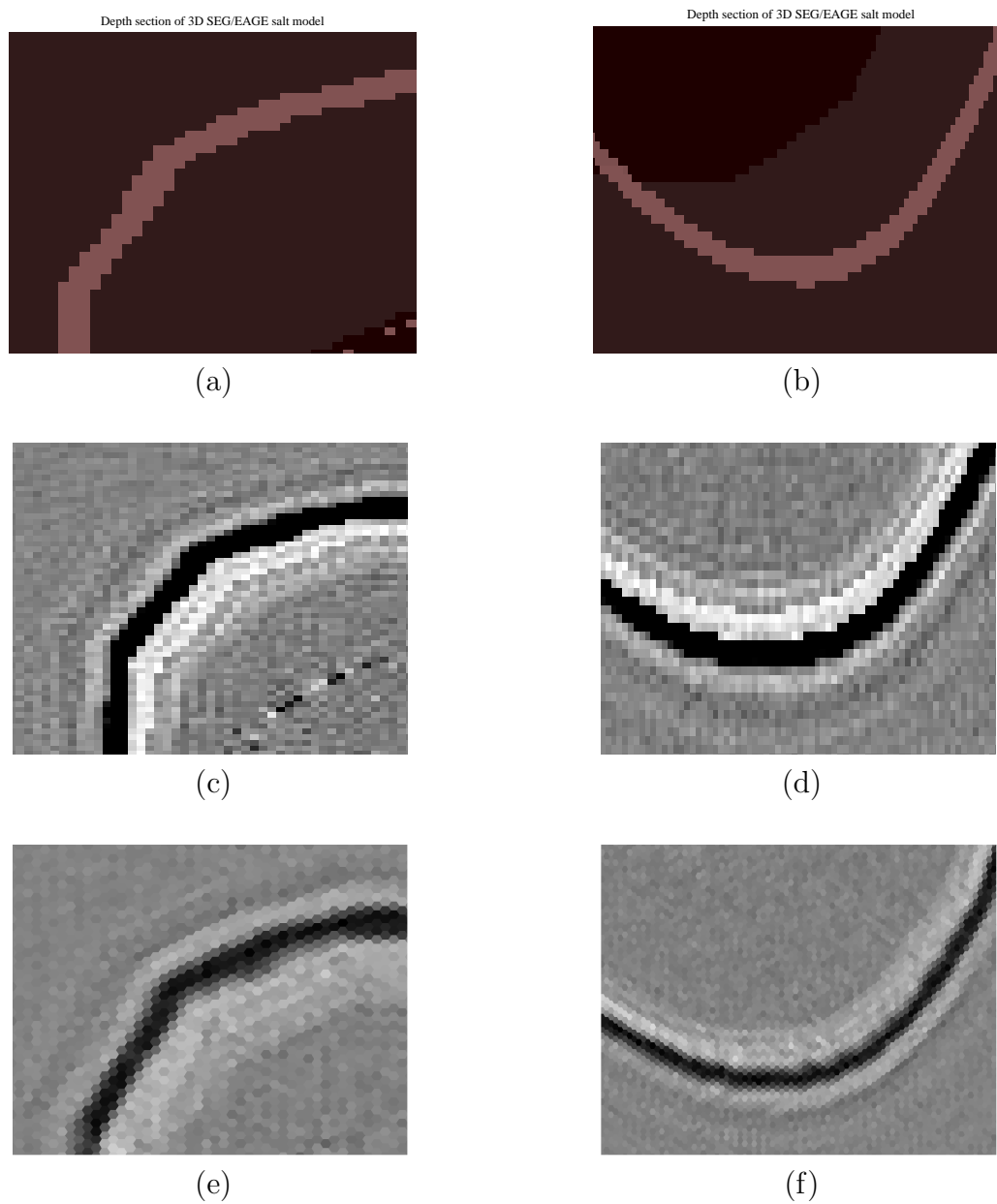


Figure 3.12: Zoomed area SEG/EAGE salt model, (a) – (b) rectangular velocity model for box-1 and box-2, (c) – (d) migrated section using rectangular PSPI, (e) – (f) migrated section using hexagonal PSPI in SA. It can be observed that hexagonal PSPI represent curves much better than rectangular version.

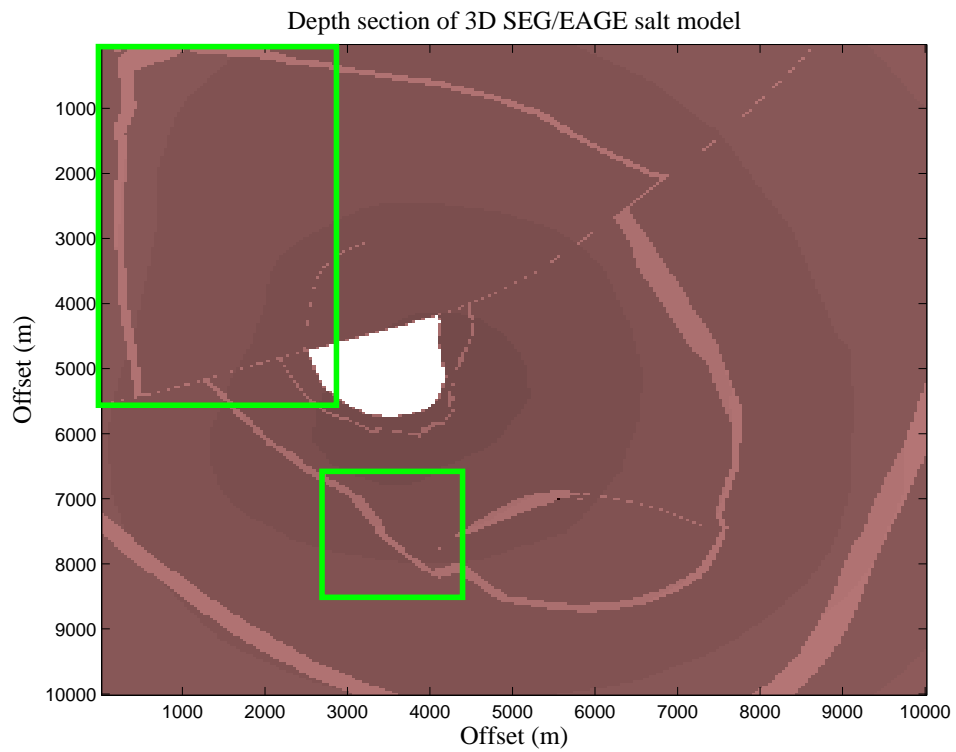


Figure 3.13: Challenging parts of the depth slice of SEG/EAGE salt model are highlighted by rectangles. The rectangle on top and bottom will be referred as box-1 and box-2 respectively.

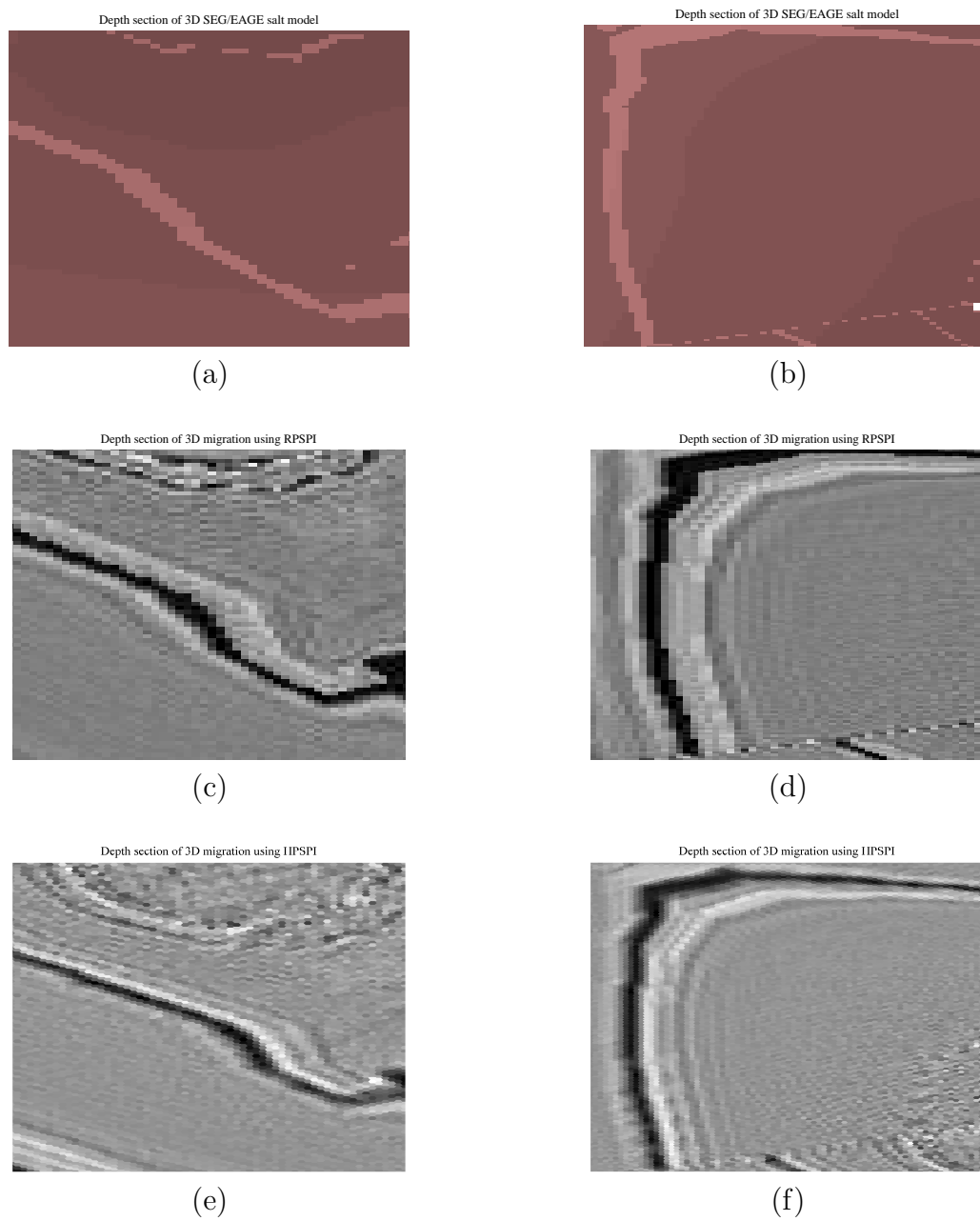


Figure 3.14: Zoomed area SEG/EAGE salt model (a) – (b) rectangular velocity model for box-1 and box-2, (c) – (d) migrated section using rectangular PSPI, (e) – (f) migrated section using hexagonal PSPI in SA.



## 3.6 Discussions

The 3D seismic data set for SEG/EAGE model was not available. Courtesy of Dr. Saleh Al-Dossary and Dr. Gino Ananos (Saudi ARAMCO), the 3D stacked seismic data for this research was obtained. The authors greatly appreciate their contribution towards this research. However, the model obtained is a down sampled version of the SEG/EAGE salt model. Further, for this research, the data has to be hexagonally sampled. The hexagonal resampling is done for each depth slice of the 3D model and seismic section. The sampling is very accurate as such, but due to the low resolution of the data, the hexagonally sampled data suffers blurring along the depth direction, as shown in the Figure 3.15. The results are subsequently effected.

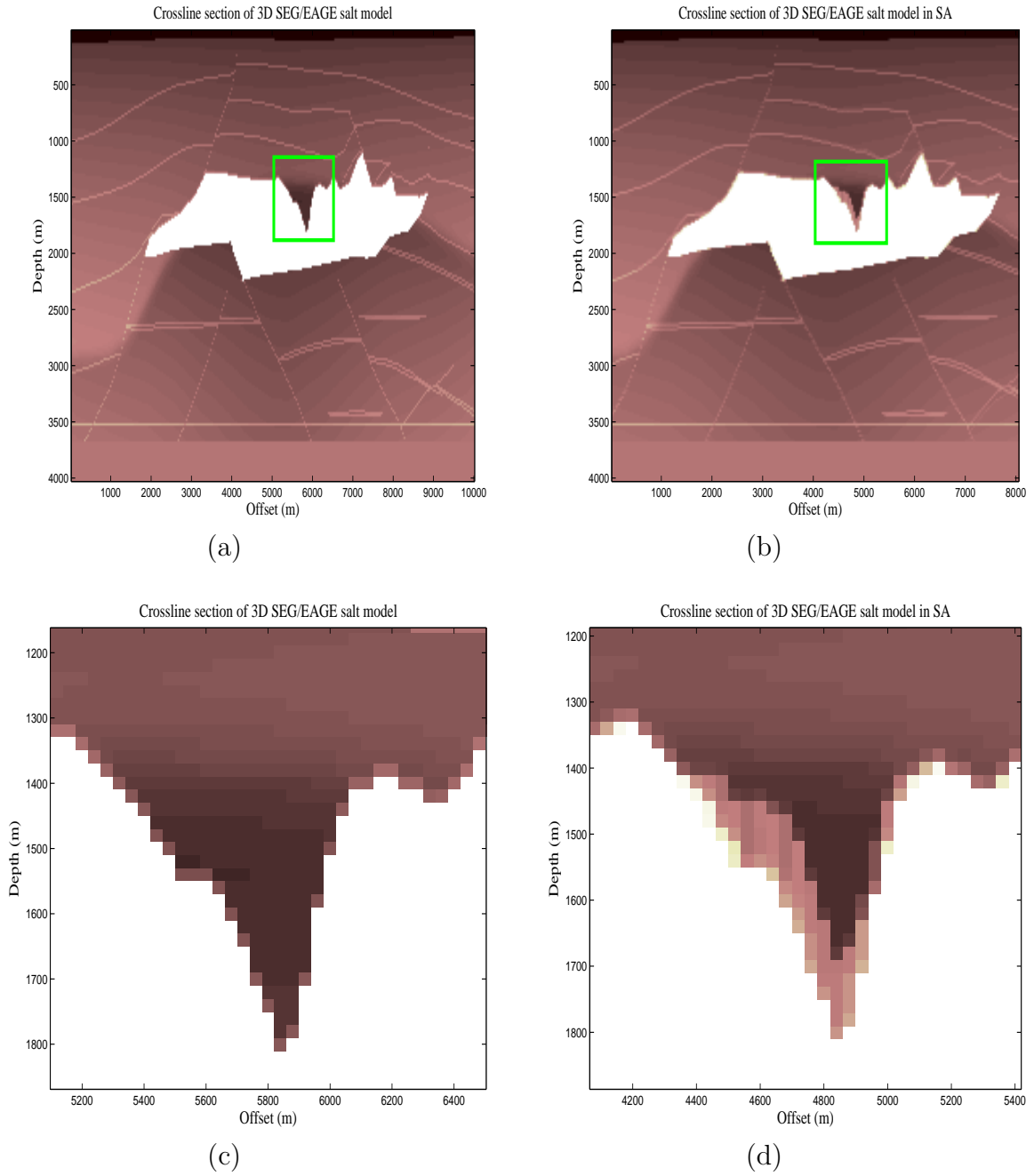


Figure 3.15: Cross-line section of SEG/EAGE salt model (a) original, (b) hexagonally sampled, (c) zoomed section of the original model, (d) zoomed section of hexagonally sampled model. The hexagonally sampled model is smeared and blurred, as the rectangular model is of low resolution.

## 3.7 Conclusions

The seismic migration techniques for hexagonally sampled data is proposed and as an example PSPI technique is used. The proposed method is shown to be efficient both in terms of time and computational savings. Further a comparison with the rectangular technique is made in terms of impulse response and migration of SEG/EAGE salt model data set. The results demonstrate that hexagonally sampled data can be easily migrated and the results are at par with the rectangular counterpart.

## CHAPTER 4

# 3D DEPTH MIGRATION USING MCCLELLAN TRANSFORMATION IN SPIRAL ARCHITECTURE

### 4.1 Introduction

High computational cost of 3D explicit depth migration has motivated researchers to propose different methods for migration of seismic data. The depth extrapolation is the important step, which constitutes to the large number of computations performed during the migration process. One of the methods proposed is to use spatially varying two-dimensional (2D) filters called as phase filters or wavefield extrapolators, which can be convolved with the data for each frequency ( $\omega$ ).

A circularly symmetric filter for depth extrapolation is given by Gazdag phase shift operator for depth extrapolation as,

$$H_d(k_x, k_y) \approx e^{(i\Delta z)} \sqrt{\left(\frac{\omega}{v}\right)^2 - (k_x^2 + k_y^2)} \quad (4.1)$$

where  $k_x$  and  $k_y$  are the inline and crossline wavenumbers respectively and  $\Delta z$  is the depth step [10]. The computational cost of convolving data with 2D filters is proportional to  $N^2$  (where N is the number of coefficients in the corresponding 1D filter). Short extrapolation filters are needed to handle strong lateral variations in the velocities accurately, while long filter lengths are required in case of steep dips. Short length filters have lesser computational requirements, thus they are more desirable. The computational cost can be reduced by splitting the 3-D extrapolation into cascade of 1-D convolutions in the inline and crossline directions, to be proportional to N. However, splitting results in errors which depend significantly on reflector dip and azimuth [56].

Hale [9] used McClellan transformations to preserve the accuracy of the 2-D extrapolation filters along with the efficiency of splitting. Using McClellan transformations symmetric 1D extrapolation filters can be converted to circularly symmetric 2D extrapolation filters. We have designed 1D wavefield extrapolators using modified projection onto convex sets [55]. McClellan transformations are an approximation to circularly symmetric filters, the accuracy can be improved

at an increasing cost of filter implementation.

Hexagonal sampling grids has been proved to be more efficient for circularly band-limited seismic data [6, 5]. In 1992, Hedley [10] proposed McClellan transformations on hexagonal grids to improve the accuracy at a reduction in the cost of implementation. However the hexagonal implementation was done based on the rectangular approach, the computational efficiency of the hexagonal sampling grid can be further improved using the spiral architecture proposed by Sheridan [16], which uses base-7 indexing for spiral addresses. Particularly the ability to represent and store a 2D data in the form of 1D vector in the spiral architecture, is the essence of its computational improvement over the rectangular approach to handle hexagonal data. Furthermore, a true hexagon is more symmetric than a rectangle, which means that quality of images for interpretation will be better.

We propose to use the hexagonal McClellan transformations on hexagonal sampling grids using the spiral architecture to further improve the computational efficiency and accuracy.

## 4.2 3D Seismic Imaging using 2D FIR Filters in SA

The depth extrapolation is performed, one angular frequency  $\omega_0$ ] at a time, using 3D extrapolation filters. The wavenumber response  $H_d(k_x, k_y)$  can be obtained from 1D wavenumber response  $H_d(k_x)$  using the McClellan transformation. The impulse response of an odd length 1-D FIR filter as proposed by McClellan and Chan [57] is:

$$H_d(k_x) = h[0] + 2 \sum_{n=1}^{\frac{N+1}{2}-1} h[n]C_n(\cos(nk)). \quad (4.2)$$

where,  $C_n(x)$  is the  $n$ th order Chebyshev polynomial in  $x$  and  $k$  is wavenumber. McClellan transformation is defined as [58]:

$$\cos(nk) = A\cos(nk_x) + B\cos(nk_y) + C\cos(nk_x)\cos(nk_y) + D = F(k_x, k_y). \quad (4.3)$$

where,  $A, B, C$  and  $D$  are filter transformation parameters. Applying Equation 4.3 to Equation 4.2, we obtain:

$$H_d(k_x, k_y) = h[0] + 2 \sum_{n=1}^{\frac{N+1}{2}-1} h[n]C_n(F(k_x, k_y)). \quad (4.4)$$

where,

$$C_n(F) = 2FCn - 1(F) - C_{n-2}(F), \quad n \geq 2 \quad (4.5)$$

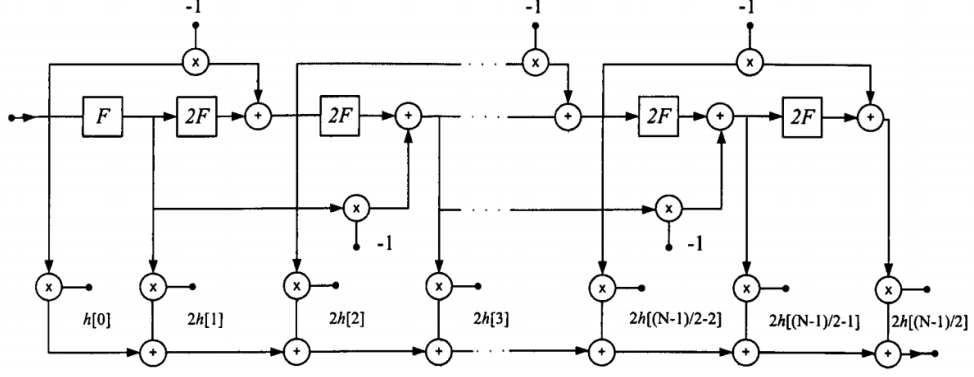


Figure 4.1: Chebyshev structure for designing 2-D FIR digital filters from 1-D odd length filters (courtesy of [8]).

The 2-D migration filters are circularly symmetric as given by Equation 4.1, these equations can be implemented by replacing  $\cos(nk)$  with  $F(k_x, k_y) = \cos(n\sqrt{kx^2 + ky^2})$  [57, 58]. An exact representation of  $F(k_x, k_y)$  is computational expensive [57]. Therefore, an approximation can be done by using  $A = B = C = -D = \frac{1}{2}$  in Equation 4.3 to obtain,

$$F(k_x, k_y) = -1 + \frac{1}{2}(1 + \cos(nk_x))(1 + \cos(nk_y)). \quad (4.6)$$

The 2-D FIR filter given by Equation 4.6 can be represented as 2-D compact FIR filter as shown in Figure 4.2 (a). However, this filter exhibits increasing error with increase in  $k$ , for  $k_x \approx k_y$ . Hale [9] improved this FIR filter design by adding extra terms to the Equation 4.6 as given by,

$$F(k_x, k_y) = -1 + \frac{1}{2}(1 + \cos(nk_x))(1 + \cos(nk_y)) - \frac{c}{2}(1 - \cos(2nk_x))(1 - \cos(2nk_y)). \quad (4.7)$$

where,  $c \approx 0.0255$  [10]. The compact 2-D improved McClellan filter given by



Equation 4.7 is shown in Figure 4.2 (b). The response of the improved McClellan filter is shown in Figure 4.6 (a).

Hedley [10] proposed the McClellan transformation approach for hexagonally sampled data. As hexagonal sampling is more efficient than rectangular sampling, with savings upto 13.4%. The hexagonal McClellan transformation filter proposed by Hedley is shown in Figure 4.3. However, the approach uses shifted rows to form a hexagon as proposed by Laine [32]. This method is not efficient and hinders the computational efficiency of hexagonal sampling scheme.

Spiral architecture (SA) proposed by Sheridan is the most efficient addressing scheme for hexagonal grids [16]. The 2-D FIR filter design in SA is more efficient as the filter coefficients can be stored and process as 1D vector. Since, the 1-D filter is symmetric and has odd length, we only process with half the coefficients, it is easier to process signals that are centered in SA than conventional cartesian method, as the spiral address index starts from the center.

Hedley proposed to sample rectangular data into hexagonal, prior to applying the FIR filters and resample data back to rectangular domain for viewing purposes. However, we propose to sample data hexagonally only once prior to the processing, as the SA data can be viewed directly without needing to revert to rectangular domain. [59].

The hexagonal McClellan filter proposed by Hedley [10] as shown in Figure 4.3, can be easily represented in spiral architecture as shown in Figure 4.4. A comparison of the filter response of the rectangular and hexagonal McClellan filter is shown in Figure 4.6. The response of hexagonal filter is more circular than the rectangular version.

### 4.3 Simulation Results

A set of 2-D hexagonal extrapolators are developed for a depth step  $\Delta z = 2$  m, in-line and cross-line  $\Delta x = \Delta y = 10$  m, time sampling interval  $\Delta t = 0.004$  s,  $\omega = 50\pi$  rad/s, and  $c = 1000$  m/s. We migrated a 3D zero-offset section with 1100 m for the in-line and cross-line apertures, up to a maximum frequency of 45 Hz. This time-space section contained one zero-phase Ricker wavelet centered at 0.512 s at  $x = y = 0$ . Figure 4.5 shows depth slices of the migrated impulse cube using Hale's McClellan filter original and improved respectively. Figure 4.7 shows the depth slices of the migrated impulse cube using the hexagonal McClellan filters in spiral architecture. The result of the hexagonal McClellan filter is sharp and more accurate than the rectangular version.

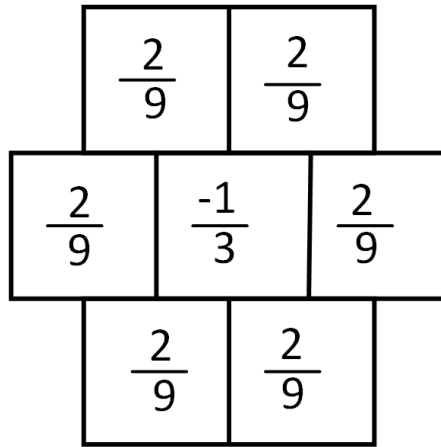
$\frac{1}{8}$	$\frac{1}{4}$	$\frac{1}{8}$
$\frac{1}{4}$	$-\frac{1}{2}$	$\frac{1}{4}$
$\frac{1}{8}$	$\frac{1}{4}$	$\frac{1}{8}$

(a)

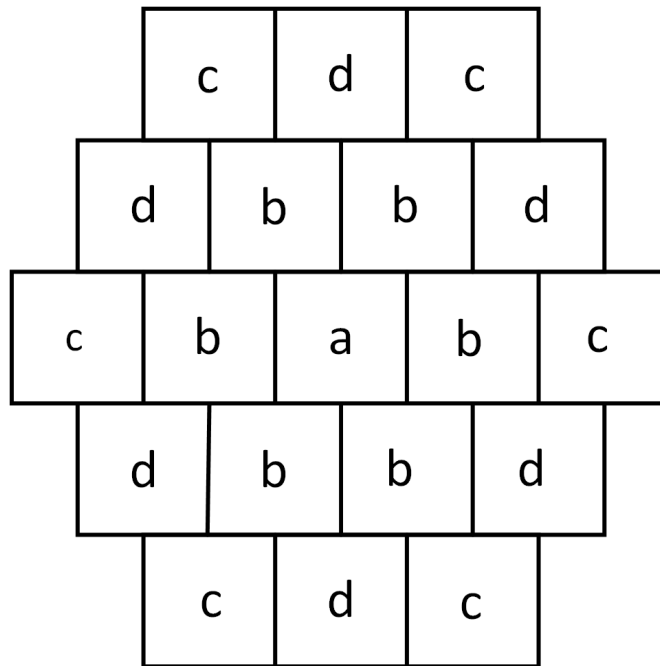
$-\frac{c}{8}$	0	$\frac{c}{4}$	0	$-\frac{c}{8}$
0	$\frac{1}{8}$	$\frac{1}{4}$	$\frac{1}{8}$	0
$\frac{c}{4}$	$\frac{1}{4}$	$-\frac{1+c}{2}$	$\frac{1}{4}$	$\frac{c}{4}$
0	$\frac{1}{8}$	$\frac{1}{4}$	$\frac{1}{8}$	0
$-\frac{c}{8}$	0	$\frac{c}{4}$	0	$-\frac{c}{8}$

(b)

Figure 4.2: Hale's McClellan transformation filter for rectangular grids (a) original, (b) improved, where  $c \approx 0.0255$  (courtesy of [9]).

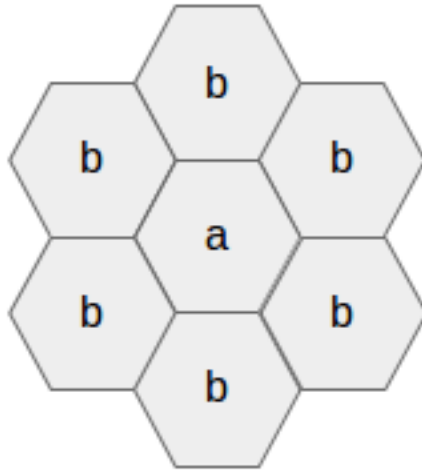


(a)

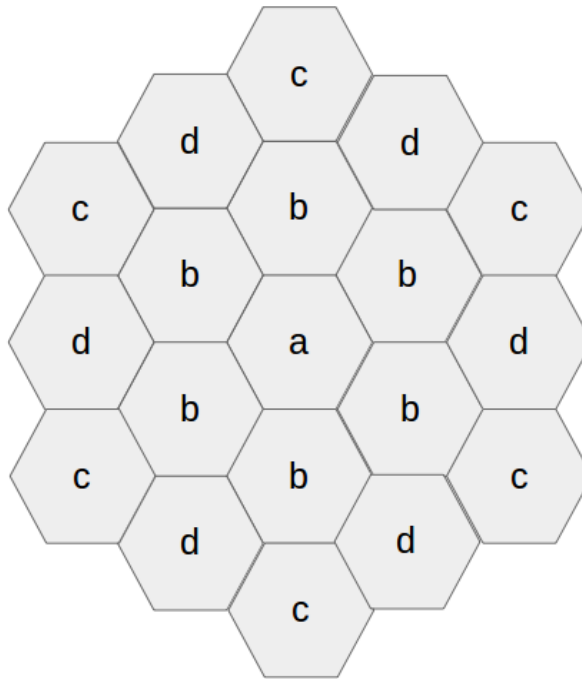


(b)

Figure 4.3: Hedley's McClellan transformation filter for hexagonal grids (a) original, (b) improved, where  $a \approx -0.708$ ,  $b \approx 0.454$ ,  $c \approx -0.00942$  and  $d \approx 0.00692$  (courtesy of [10]).

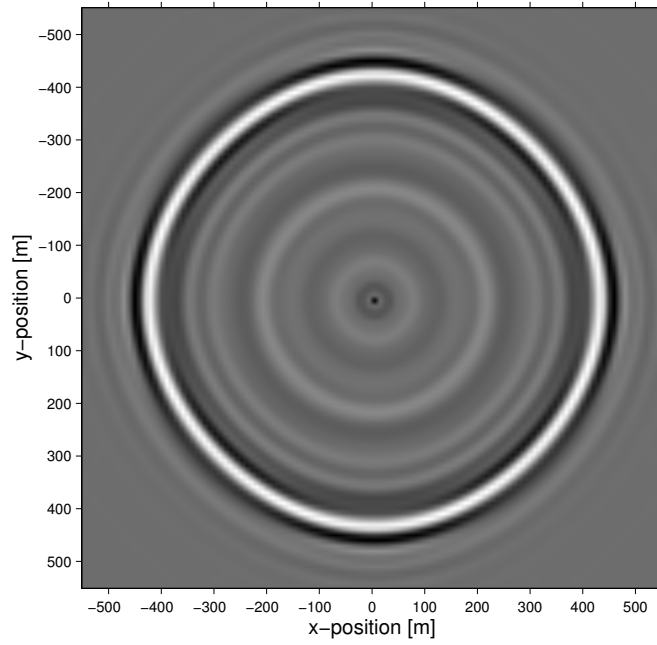


(a)

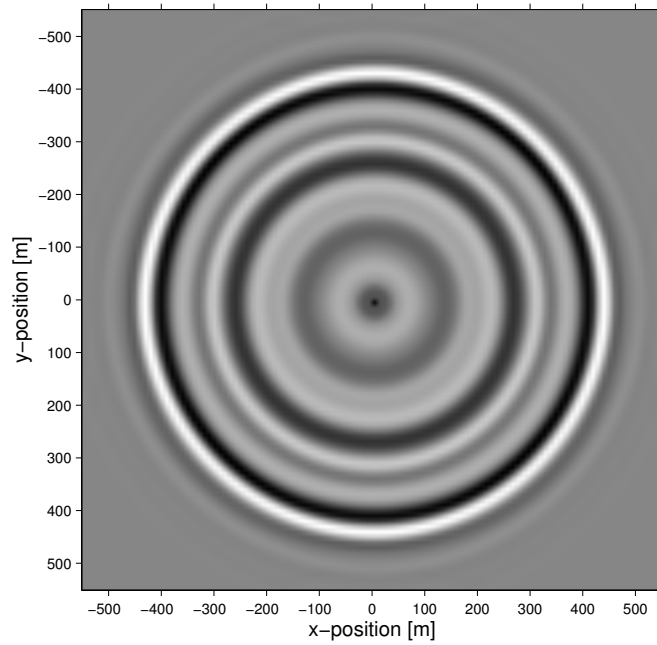


(b)

Figure 4.4: Proposed McClellan transformation filter for hexagonal grids in SA  
 (a) original, where  $a \approx -0.333$ ,  $b \approx 0.222$ , (b) improved, where  $a \approx -0.354$ ,  
 $b \approx 0.227$ ,  $c \approx -0.00471$  and  $d \approx 0.00346$ .

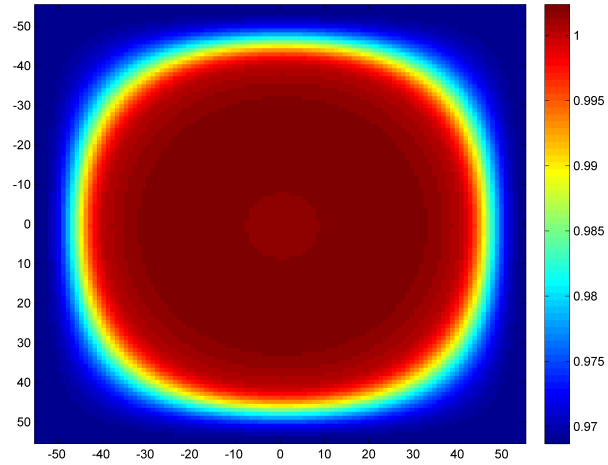


(a)

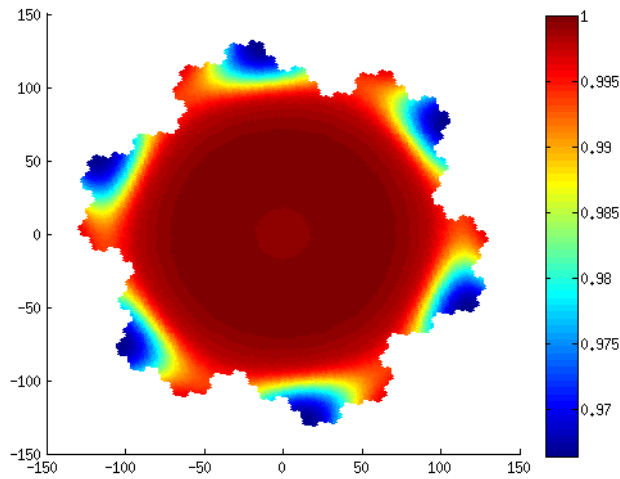


(b)

Figure 4.5: Depth slice of the 3D seismic migration of impulse response using Hale-McClellan transformation filter (a) original, (b) improved.



(a)



(b)

Figure 4.6: 2D Filter response (a) improved McClellan transformation as in [9] ,  
 (b) proposed improved McClellan transformation in SA.

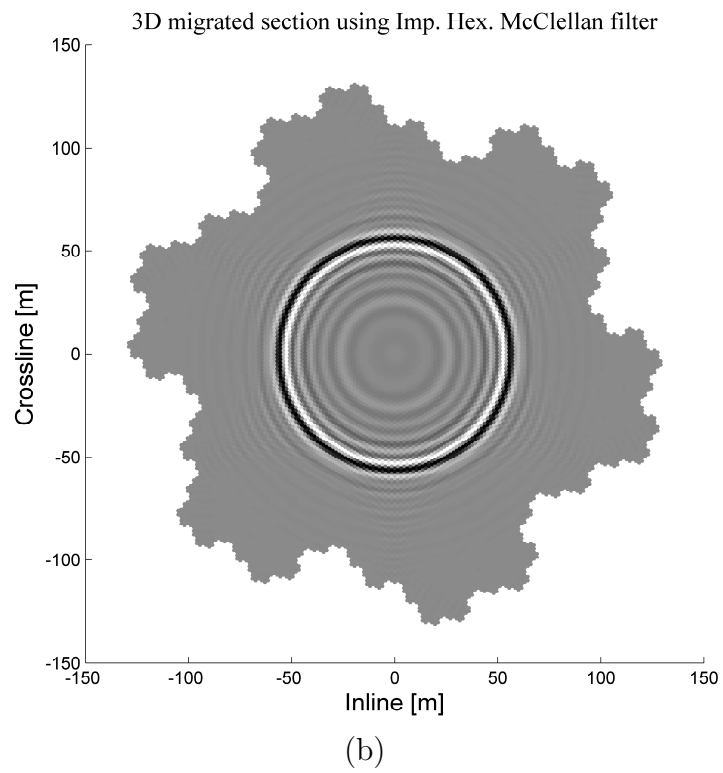
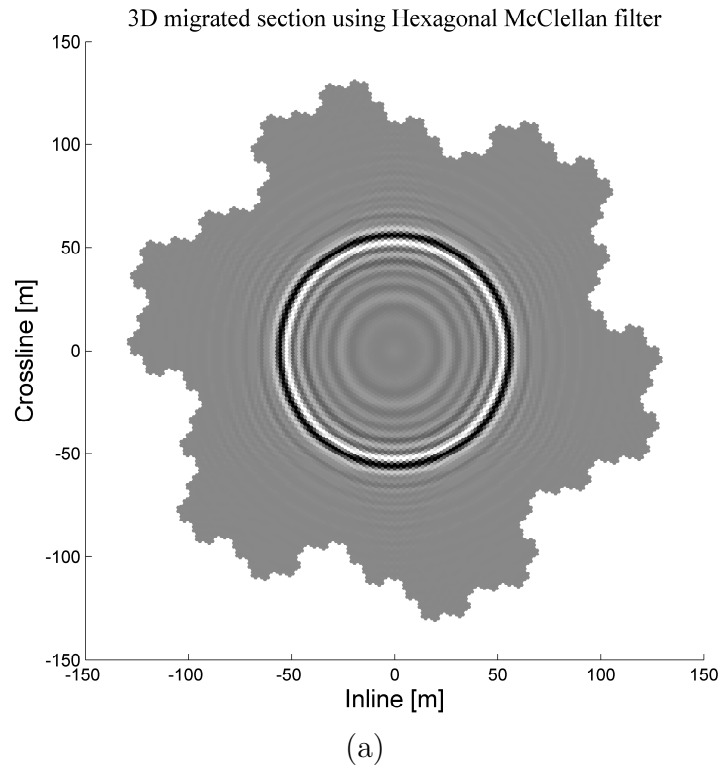


Figure 4.7: Depth slice of the 3D seismic migration of impulse response using proposed McClellan transformation filter in SA (a) original, (b) improved.



## 4.4 Conclusions

McClellan Transformation filters in spiral architecture have been implemented and tested. An impulse cube is migrated using the original and improved McClellan filter in rectangular and spiral architecture. The migration results of hexagonal McClellan transformation is much better than the rectangular counterpart. The computational requirement using the spiral architecture is much less than the rectangular technique, with better quality of images.

## CHAPTER 5

# CONCLUSIONS

In this research work, the computational complexity of handling huge seismic data is considered and solved using the hexagonal sampling technique, for proof of concept Phase Shift Plus Interpolation (PSPI) migration is performed on the impulse cube and the benchmark 3D SEG/EAGE dataset. The results are better for depth slices in the hexagonal scheme. The imaging for the in-line and cross-line sections is very close to the rectangular version. The quality of HPSPI migrated section of the SEG/EAGE salt model suffers because of blurring of the hexagonally sampled input seismic data. The shown clearly in Figure 3.15

Open source hexagonally acquired seismic data was not available. It would take a very long time and effort to create a seismic data section with hexagonal grids, the rectangular data was hexagonally sampled and used, to prove the concept of the proposed technique. Better results can be obtained when the data is truly acquired using hexagonal grids.

Furthermore, in this thesis, stable extrapolators are designed, for explicit depth extrapolation of 3D wavefields using McClellan transformation filters in spiral architecture.

## 5.1 Future Works

This work can be extended for the prestack imaging of the seismic data for better quality of the images, without any limitations. Since the resampling of the seismic data is not ideal, seismic data generation should be done using hexagonal grids prior to applying hexagonal migration techniques.

Reverse Time Migration (RTM) is more computationally expensive than PSPI and yields imaging with better accuracy in complex geological conditions. It would be interesting to see the RTM imaging in hexagonal grids using spiral architecture.

Furthermore, sparse FIR filters can be used to image seismic data using hexagonal spiral architecture. Sparse filters can further reduce the computational time. Since, the computational time for algorithms coded in lower level languages (than MATLAB) is less, hexagonal migration codes can be easily ported to languages such as C, Python, etc. which would be essential for Prestack imaging as the time required would grow exponentially.

# REFERENCES

- [1] A. Cordsen, M. Galbraith, J. Peirce, and B. A. Hardage, *Planning land 3-D seismic surveys*. Society of exploration geophysicists Tulsa, 2000, vol. 9.
- [2] B. Biondi, *3D seismic imaging*. Society of Exploration Geophysicists Tulsa, 2006, vol. 14.
- [3] J. B. Bednar, “Modeling, Migration and Velocity Analysis in Simple and Complex Structure,” *by Panorama Technologies, Inc*, 2009.
- [4] L. Middleton and J. Sivaswamy, *Hexagonal Image Processing : A Practical Approach*, 2005, vol. 224, no. 4. [Online]. Available: <http://eprints.soton.ac.uk/262819/>
- [5] R. M. Mersereau, “The processing of hexagonally sampled two-dimensional signals,” *Proceedings of the IEEE*, vol. 67, no. 6, pp. 930–949, 1979.
- [6] V. Bardan, “A hexagonal sampling grid for 3D recording and processing of 3D seismic data,” *Geophysical Prospecting*, vol. 45, no. 5, pp. 819–830, 1997. [Online]. Available: <http://doi.wiley.com/10.1046/j.1365-2478.1997.600300.x>

- [7] H. Ashraf, “Efficient Approach For Processing of Hexagonally Sampled Exploration Seismic Data,” *M.S. Thesis, King Fahd University of Petroleum and Minerals*, March, 2015.
- [8] W. A. Mousa, “Frequency-space wavefield extrapolation using infinite impulse response digital filters: is it feasible?” *Geophysical Prospecting*, vol. 61, no. 3, pp. 504–515, 2013. [Online]. Available: <http://doi.wiley.com/10.1111/j.1365-2478.2012.01058.x>
- [9] D. Hale, “3-D depth migration via McClellan transformations,” *Geophysics*, vol. 56, no. 11, pp. 1778–1785, 1991. [Online]. Available: <http://library.seg.org/doi/abs/10.1190/1.1442990>
- [10] J. P. Hedley, “3-D migration via McClellan transformations on hexagonal grids,” *Geophysics*, vol. 57, no. 8, p. 1048, Aug 1992. [Online]. Available: <http://library.seg.org/doi/abs/10.1190/1.1443316>
- [11] Ö. Yilmaz, *Seismic Data Analysis: Processing, Inversion, and Interpretation of Seismic Data*, 2001, vol. 10. [Online]. Available: <http://library.seg.org/doi/book/10.1190/1.9781560801580>
- [12] R. Bording and L. Lines, *Seismic Modeling and Imaging with the Complete Wave Equation*, 1997. [Online]. Available: <http://dx.doi.org/10.1190/1.9781560801870>

- [13] G. V. Keller, "An introduction to geophysical exploration," *Eos, Transactions American Geophysical Union*, vol. 67, no. 11, pp. 132–132, 1986. [Online]. Available: <http://dx.doi.org/10.1029/EO067i011p00132-01>
- [14] M. Lansley, "Shifting paradigms in land data acquisition," *first break*, vol. 31, no. 1, 2013.
- [15] R. Mersereau, "Two-dimensional signal processing from hexagonal rasters," *ICASSP '78. IEEE International Conference on Acoustics, Speech, and Signal Processing*, vol. 3, 1978.
- [16] P. Sheridan, "Spiral Architecture for Machine Vision," *Thesis, University of Technology, Sydney*, 1996.
- [17] W. K. Aylor, "Business performance and value of exploitation 3-D seismic," *The Leading Edge*, vol. 14, no. 7, pp. 797–801, 1995.
- [18] G. T. Schuster, *Basics of Seismic Imaging*, 2010, no. Isbn 9780521871242.
- [19] S. H. Gray, J. Etgen, J. Dellinger, and D. Whitmore, "Seismic migration problems and solutions," *Geophysics*, vol. 66, no. 5, pp. 1622–1640, 2001.
- [20] R. Mittet, "A simple design procedure for depth extrapolation operators that compensate for absorption and dispersion," *Geophysics*, vol. 72, no. 2, p. S105, 2007.
- [21] J. Attanayake, "Seismic Migration ( SM ) Goals," 2006.

- [22] R. Carbonell, *Exploration seismology*. Cambridge university press, 1997, vol. 271.
- [23] R. Stolt, “Migration by fourier transform,” *Geophysics*, vol. 43, no. 1, pp. 23–48, 1978.
- [24] J. Gazdag, “Migration of seismic data by phase shift plus interpolation,” *Geophysics*, vol. 49, p. 124, 1984.
- [25] J. C. Bancroft, “Review of seismic imaging : Prestack,” *Geophysics*, vol. 13, pp. 551–571, November, 2001.
- [26] R. A. Bale, S. H. Gray, and M. G. K. Grech, “TTI wave equation migration by phase-shift plus interpolation,” *CGGVeritas, Calgary, Canada*, 2007.
- [27] J. Pan and D. Negut, “A phase shift plus interpolation algorithm for prestack time migration,” *SEG Technical Program Expanded Abstracts 2008*, pp. 2407–2411, jan 2008. [Online]. Available: <http://library.seg.org/doi/abs/10.1190/1.3059362>
- [28] H. D. Geiger and G. F. Margrave, “Automatic selection of reference velocities for recursive depth migration,” *CREWES Research Report*, vol. 16, no. 1992, pp. 1–9, 2004.
- [29] L. Dan, Y. Xiao, P. Cheng, G. Wu, and S. Li, “A low-complexity multiple signal representation scheme in downlink OFDM-CDMA,” *Science in China Series F: Information Sciences*, vol. 52, no. 12, pp. 2433–2444, 2009. [Online]. Available: <http://link.springer.com/10.1007/s11432-009-0211-9>

- [30] J.-B. Chen and S.-Y. Du, “Kinematic characteristics and the influence of reference velocities of phase-shift-plus-interpolation and extended-split-step-Fourier migration methods,” *Geophysical Prospecting*, vol. 58, no. 3, pp. 429–439, may 2010. [Online]. Available: <http://doi.wiley.com/10.1111/j.1365-2478.2009.00845.x>
- [31] B. Qiao and J. C. Bancroft, “Choosing reference velocities for PSPI migration,” *CREWES Research Report*, vol. 21, no. 3, pp. 1–8, 2009.
- [32] A. F. Laine, S. Schuler, W. Huda, J. C. Honeyman-Buck, and B. G. Steinbach, “Hexagonal wavelet processing of digital mammography,” vol. 1898, 1993, pp. 559–573. [Online]. Available: <http://dx.doi.org/10.1117/12.154543>
- [33] I. Her, “Geometric transformations on the hexagonal grid.” *IEEE transactions on image processing*, vol. 4, no. 9, pp. 1213–22, 1995. [Online]. Available: <http://www.ncbi.nlm.nih.gov/pubmed/18292018>
- [34] P. J. Burt, “Tree and pyramid structures for coding hexagonally sampled binary images,” *Computer Graphics and Image Processing*, vol. 14, no. 3, pp. 271–280, 1980. [Online]. Available: <http://linkinghub.elsevier.com/retrieve/pii/0146664X80900568>
- [35] Y. Liu and H. Ma, “Reliable cooperative spectrum sensing based on double threshold detection and Dempster-Shafer theory,” *2012 IEEE 11th International Conference on Sig-*



- nal Processing*, pp. 1536–1540, oct 2012. [Online]. Available: <http://ieeexplore.ieee.org/lpdocs/epic03/wrapper.htm?arnumber=6491866>
- [36] C. Bagaini, E. Bonomi, and E. Pieroni, “Data parallel implementation of 3d pspi,” *SEG Annual Meeting, 8-13 October, Houston, Texas*, 1995.
- [37] J. P. Hedley, “3-D migration via McClellan transformations on hexagonal grids,” *Geophysics*, vol. 57, no. 8, p. 1048, 1992.
- [38] A. Ozbek, L. Hoteit, and G. Dumitru, “3D filter design on a hexagonal grid with applications to point-receiver land acquisition,” *74th Ann. Internat. Mtg.*, no. October, pp. 1965–1968, 2004.
- [39] S. Gesbert, C. Haneveld, and S. Saleh, “3D hexagonal prestack depth migration of seismic data,” *The Leading Edge*, vol. 26, p. 1262, 2007.
- [40] B. Hamilton and S. Bilbao, “Hexagonal vs. rectilinear grids for explicit finite difference schemes for the two-dimensional wave equation,” *The Journal of the Acoustical Society of America*, vol. 133, no. 5, p. 3532, 2013. [Online]. Available: <http://scitation.aip.org/content/asa/journal/jasa/133/5/10.1121/1.4806369>
- [41] V. Bardan, “Hexagonal sampling and hexagonal binning in 3D seismic data acquisition,” *72nd Ann. Internat. Mtg*, vol. 21, no. March, pp. 1392–1395, 2002.

- [42] M. Woodward and F. Muir, “Hexagonal Finite Difference Operators and 3-D Wave Equation Migration,” Stanford Exploration Project, SEP-38, Tech. Rep., 1984.
- [43] M. Woodward and N. Moldoveanu, “Binning of three dimensional seismic data,” Patent, U.S. Patent Documentation, 1999.
- [44] A. Ozbek, L. Hoteit, and G. Dumitru, “3D filter design on a hexagonal grid with applications to point-receiver land acquisition,” *74th Ann. Internat. Mtg.*, no. October, pp. 1965–1968, 2004.
- [45] S. Gesbert, C. Haneveld, and S. Saleh, “3D “hexagonal” prestack depth migration of seismic data,” *The Leading Edge*, vol. 26, no. 10, pp. 1262–1265, 2007.
- [46] X. He and W. Jia, “Hexagonal Structure for Intelligent Vision,” *First International Conference on Information and Communication Technologies (ICICT 2005)*, pp. 52–64.
- [47] R. C. Staunton and N. Storey, “A comparison between square and hexagonal sampling methods for pipeline image processing,” *Proc. of SPIE Medical Imaging*, 1989.
- [48] I. Her, “Geometric transformations on the hexagonal grid,” *IEEE Transactions on Image Processing*, vol. 4, no. 9, pp. 1213–1222.
- [49] R. Staunton, “Hexagonal image sampling: a practical proposition,” in *Proc. SPIE Vol. 1008, p. 23, Expert Robots for Industrial Use, David P. Casasent*;

- Ernest L. Hall; Kenneth J. Stout; Eds.*, ser. Presented at the Society of Photo-Optical Instrumentation Engineers (SPIE) Conference, vol. 1008, 1988.
- [50] W. E. Snyder, H. Qi, and W. Sender, “A coordinate system for hexagonal pixels,” *Proc. of SPIE Medical Imaging*, 1999.
- [51] A. Rosenfeld and J. L. Pfaltz, “Distance functions on digital pictures,” *Pattern recognition*, vol. 1, no. 1, pp. 33–61, 1968.
- [52] J. Serra, “Introduction to mathematical morphology,” *Computer vision, graphics, and image processing*, vol. 35, no. 3, pp. 283–305, 1986.
- [53] S. A. Levin, “ $\Delta x \neq \Delta y$  in 3D depth migration via McClellan transformations,” *Geophysical Prospecting*, vol. 52, no. 3, pp. 241–246, 2004.
- [54] W. A. Mousa, “Design and Implementation of Complex-Valued FIR Digital Filters with Application to Migration of Seismic Data,” Ph.D. dissertation, University of Leeds, 2006.
- [55] W. A. Mousa, M. van der Baan, S. Boussakta, and D. C. McLernon, “Designing stable extrapolators for explicit depth extrapolation of 2D and 3D wavefields using projections onto convex sets,” *Geophysics*, vol. 74, no. 2, p. S33, 2009.
- [56] D. L. Brown, “Applications of operator separation in reflection seismology,” *Geophysics*, vol. 48, no. 3, pp. 288–294, 1983.

- [57] S. K. Chan and J. H. McClellan, “A 2-D FIR Filter Structure Derived from the Chebyshev Recursion,” *Circuits and Systems , IEEE Transactions on*, vol. C, no. July, pp. 372–378, 1977.
- [58] W. F. Mecklenbräuker and R. M. Mersereau, “McClellan transformations for Two-Dimensional Digital Filtering: II implementation,” *IEEE Trans. on Circuits and Systems*, vol. 23, no. 7, pp. 414–422, 1976.
- [59] S. Bobe, “Image registration on a hexagonal lattice,” Ph.D. dissertation, University of Applied Sciences, Bielefeld, 2007.

# Vitae

- Name: Mohammed Shahabuddin
- Nationality: Indian
- Date of Birth: 12<sup>th</sup> April 1989
- Email: *shahabuddin.mjcet@gmail.com*
- Permanent Address: 23-2-240, Near Volta Hotel, Moghalpura, Hyderabad,  
India
- Bachelor's Degree: Osmania University, Hyderabad, India.